





## Research Article

# Synthesis, Antibacterial, and Antioxidant Activities of Thiazolyl-Pyrazoline Schiff Base Hybrids: A Combined Experimental and Computational Study

Demis Zelelew <sup>1</sup>, Milkyas Endale <sup>1</sup>, Yadessa Melaku <sup>1</sup>, Fedlu Kedir <sup>1</sup>,  
Taye B. Demissie <sup>2</sup>, Japheth O. Ombito <sup>2</sup> and Rajalakshmanan Eswaramoorthy <sup>3</sup>

<sup>1</sup>Department of Applied Chemistry, School of Applied Natural Science, Adama Science and Technology University, P.O. Box 1888, Adama, Ethiopia

<sup>2</sup>Department of Chemistry, University of Botswana, P/Bag UB 00704, Gaborone, Botswana

<sup>3</sup>Department of Biomaterials, Saveetha Dental College and Hospital, Saveetha University, Chennai 600 077, India

Correspondence should be addressed to Milkyas Endale; milkyasendale@yahoo.com

Received 5 July 2022; Accepted 3 September 2022; Published 27 September 2022

Academic Editor: Liviu Mitu

Copyright © 2022 Demis Zelelew et al. This is an open access article distributed under the Creative Commons Attribution License, which permits unrestricted use, distribution, and reproduction in any medium, provided the original work is properly cited.

Thiazole-pyrazoline Schiff base hybrids have a broad range of pharmacological potential with an ability to control the activity of numerous metabolic enzymes. In this work, a greener and more efficient approach has been developed to synthesize a novel series of thiazole-pyrazoline Schiff base hybrids using ZnO nanoparticle-assisted protocol in good to excellent yields (78.3–96.9%) and examined their antibacterial activity against Gram-positive and Gram-negative bacteria, as well as their antioxidant activity. Compound 24 (IZD =  $18.67 \pm 0.58$ ) displayed better activity against *P. aeruginosa* compared with amoxicillin (IZD =  $14.33 \pm 2.52$ ) at 250  $\mu\text{g/mL}$ , whereas compounds 22 and 24 (IZD =  $13.33 \pm 0.58$  mm and  $17.00 \pm 1.00$  mm, respectively) showed better activity against *E. coli* compared with amoxicillin (IZD =  $14.67 \pm 0.58$  mm) at 500  $\mu\text{g/mL}$ . The remaining compounds showed moderate to weak activity against the tested bacterial strains. Compound 21 displayed significant inhibition of DPPH ( $\text{IC}_{50} = 4.63 \mu\text{g/mL}$ ) compared with ascorbic acid ( $\text{IC}_{50} = 3.21 \mu\text{g/mL}$ ). Compound 21 displayed 80.01  $\pm$  0.07% inhibition of peroxide formation, suggesting its potential in preventing the formation of lipid peroxides. The results of the ADMET study showed that all synthesized compounds obeyed Lipinski's rule of five. *In silico* pharmacokinetic study demonstrated that compound 24 had superior intestinal absorption compared with amoxicillin. *In silico* molecular docking analysis revealed a binding affinity of  $-9.9$  Kcal/mol for compound 24 against PqsA compared with amoxicillin ( $-7.3$  Kcal/mol), whereas compounds 22 and 24 displayed higher binding affinity ( $-8.5$  and  $-7.9$  Kcal/mol, respectively) with DNA gyrase B compared with amoxicillin ( $-7.1$  Kcal/mol), in good agreement with *in vitro* antibacterial activity against *P. aeruginosa* and *E. coli*. *In silico* toxicity study showed that all synthesized compounds had  $\text{LD}_{50}$  (mg/kg) values ranging from 800 to 1,000 putting them in ProTox-II class 4. The *in vitro* antibacterial activity and molecular docking analysis showed that compound 24 is a promising antibacterial therapeutic agent against *P. aeruginosa* and *E. coli* and compound 22 is a promising antibacterial agent against *E. coli*, whereas compound 21 is found to be a potential natural antioxidant agent. Moreover, the green synthesis approach using ZnO nanoparticle as catalyst was found to be a very efficient method to synthesize biologically active thiazole-pyrazoline Schiff base hybrids compared with the conventional method.

## 1. Introduction

Antimicrobial resistance (AMR) poses a major threat to human health around the world [1]. In recent years, attention has been given to the development of treatments that generate oxidative stress as part of their antibacterial

mechanism of action [2]. Therefore, there is an imperative need to search for antimicrobials with antioxidant and antibacterial properties to counter the problems of bacterial resistance. A molecular hybridization is a valuable approach for the design and development of new biological molecules in which two or more active pharmacophoric units are

combined to form a new hybrid molecule with increased potency [3, 4].

For many decades, thiazole and pyrazoline scaffolds have been studied extensively and found to possess a wide range of chemical reactivity and pharmacological activities [5, 6]. These five-membered heterocyclic compounds have been proven to possess antibacterial activity and the ability to delocalize free radicals and produce stable DPPH fragments [7]. In addition to antibacterial activity, thiazole derivatives exhibit antimicrobial [8], antiviral [9], antidiabetic [10], anticonvulsant [11], antioxidant [12], anti-HIV [13], anti-inflammatory [14], Alzheimer's disease [15], and antitumor activities [16]. Previous studies revealed that 3,5-diaryl-4,5-dihydro-1*H*-pyrazole derivatives, which are members of the 2-pyrazoline class, have been extensively investigated using a variety of structural manipulations and it has been discovered that the steric and electronic properties of the various substituents at the N-1, C-3, and C-5 positions, as well as the chirality aspects of these molecules, have a critical influence on activity [17]. The N-N bond link of the pyrazoline ring is thought to be important in their biological activity [18]. Zinc oxide nanoparticle is gaining popularity as a heterogeneous catalyst for a variety of organic transformations due to their low cost, nontoxicity, waste reduction, and recycling properties [19]. The impressive catalytic ability of ZnO nanoparticles associated with morphology-tuned specific microstructures, ability of electron transportation, and their high stability when combined with the intrinsic Lewis acid of the zinc ion motivated us to consider this catalyst.

In the present work, we hereby present ZnO nanoparticle-assisted synthesis of nine novel thiazolyl-pyrazoline Schiff base hybrids, *in vitro* antibacterial and antioxidant activity along with molecular docking studies, *in silico* ADMET prediction, drug-likeness, and pharmacokinetic and toxicity properties.

## 2. Materials and Methods

All starting chemicals and materials used were analytical grades. Merck (Germany), Sigma-Aldrich Sigma Chemical, Co. (USA), and Loba Chemie, Pvt Ltd. (India) provided preliminary chemicals and reagents, which were purchased from commercial vendors and used immediately without additional purification unless otherwise noted. Column chromatography was performed using (Merck) silica gel (particle size 60–120 mm) with *n*-hexane, ethyl acetate, and dichloromethane as mobile phase. ZnO nanoparticles were obtained from the Department of Applied Chemistry, Material Chemistry Research Team of ASTU, which is characterized by UV-vis and FT-IR spectroscopy, X-ray diffraction (XRD), transmission electron microscopy (TEM), photoluminescence (PL), and thermogravimetric analysis (TGA) techniques [20]. Amoxicillin and *L*-ascorbic acid (99%) were employed as standards, both obtained from Ethiopian Pharmaceutical Manufacturing Factory (EPHARM).

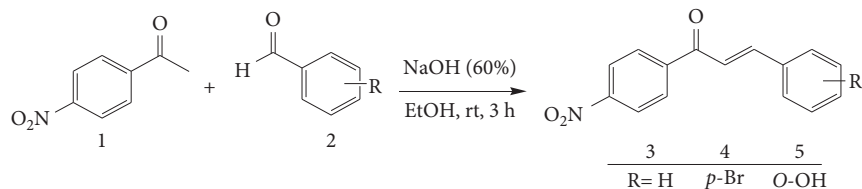
Melting points were determined on a Gallenkamp MFB-595 apparatus, uncorrected. UV spectra were obtained using a double-beam UV-visible spectrophotometer (Model 2201,

India). The <sup>1</sup>H-NMR and <sup>13</sup>C-NMR spectra were recorded at 400 and 100 MHz, respectively, on a Bruker Avance III 400 Nanospectrometer using tetramethylsilane (TMS) as an internal standard. The chemical shifts are expressed in δ (ppm) and reported as s (singlet), d (doublet), t (triplet), q (quartet), m (multiplet), dd (doublet of doublets), and brs (broad singlet), respectively. Analytical TLC analysis was performed on pre-coated aluminum plate silica gel 60 F<sub>254</sub> (Merck, Darmstadt, Germany). Detection was carried out under UV light (254 and 365 nm). Column chromatographic separations were carried out on silica gel (60–120 mesh, Merck). SwissADME and AutoDock Vina 4.2.6 version software packages were used to undertake *in silico* ADMET and molecular docking simulation investigations, respectively.

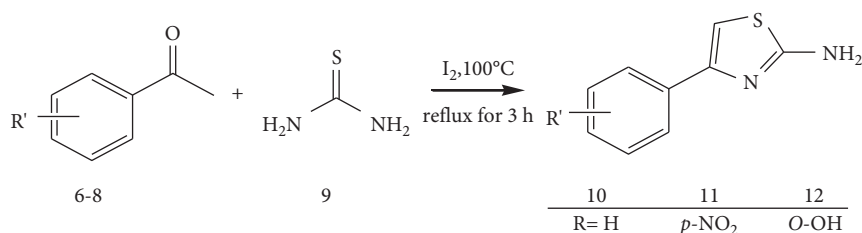
### 2.1. Synthesis Procedures

**2.1.1. Synthesis of Chalcones (1, 3-Diaryl-2-propen-1-ones, 3–5).** To an equimolar amount of *p*-nitro acetophenone (1, 0.06 mol) and the corresponding aldehyde derivatives (2, 0.06 mol) in 5–10 mL of ethanol, 60% (w/v) NaOH was added dropwise (3 mL) and stirred for 30 min (Scheme 1 and SI Appendix A Figure S1) [21]. The resulting solid products (5–7) were stirred in an ice bath for 30 min and then at RT until the precipitate was formed within 3 h. The reaction progress was monitored by TLC with an eluent of *n*-hexane: ethyl acetate (9:1). The precipitate was filtered off and washed thoroughly with cold distilled water and cold methanol (2 × 20 mL). The products (5–7) were recrystallized from absolute ethanol to yield a yellow precipitate of chalcone derivatives.

**2.1.2. Synthesis of 2-Amino-4-(substituted-phenyl)-1, 3-thiazole Derivatives (10–12).** The thiazole moiety was synthesized by utilizing Hantzsch's modified approach (Scheme 2), which involved a solvent-free reaction of substituted acetophenone (6–8) derivatives with thiourea (9) and iodine under thermal conditions resulting in 2-amino-4-aryl thiazole derivatives (10–12, SI Appendix A, Figure S2) [22]. Thiourea (40 mmol, 2 molar equiv.) was mixed with iodine beads (20 mmol, 1 molar equiv.) in a mortar, and the mixture was homogenized with a pestle. The solids were scratched off into a 250 mL round-bottom flask with a magnetic stirring bar and charged with the corresponding acetophenone (20 mmol, 1 molar equiv.). The flask was heated in an oil bath under an air-cooled condenser at 100°C with stirring. The reaction progress was monitored using TLC in *n*-hexane and ethyl acetate (4:1). After 3 hours, the mixture was cooled and it solidified again. A saturated aqueous solution of sodium thiosulfate (Na<sub>2</sub>S<sub>2</sub>O<sub>3</sub>·5H<sub>2</sub>O, 5%) was added with concomitant mechanical disruption of the solid matrix in a sufficient amount to reduce the remaining iodine. The product as a suspension was filtered off and carefully washed with 20 mL of diethyl ether to remove the residues of unreacted acetophenone. The crude product was dissolved in hot water, filtered, and the hot filtrate was adjusted to pH = 9 by aqueous NaHCO<sub>3</sub>. After cooling, the precipitated product was collected and recrystallized using ethanol.



SCHEME 1: Synthesis of chalcone derivatives (3–5).



SCHEME 2: Synthesis of 2-amino-4-(substituted-phenyl)thiazole derivatives (10–12).

4-Phenylthiazol-2-amine (10). White solid powder; yield: 96.6%; m.p.: 144–146°C;  $R_f$  (20% EtOAc in *n*-hexane) = 0.61;  $^1\text{H-NMR}$  (400 MHz,  $\text{DMSO-}d_6$ ):  $\delta$  7.35 (d,  $J = 7.7$  Hz, 2H, ArH), 6.94 (t,  $J = 7.6$  Hz, 2H, ArH), 6.84 (d,  $J = 7.3$  Hz, 1H, ArH), 6.55 (s, 1H, CH of thiazole), 2.1 (d, 2H,  $-\text{NH}_2$ );  $^{13}\text{C-NMR}$  (100 MHz,  $\text{DMSO-}d_6$ ):  $\delta$  168.7, 150.2, 135.1, 128.9, 127.7, 125.9, 102.0.

4-(4-Nitrophenyl)thiazol-2-amine (11). Orange solid powder; yield: 86.6%; m.p.: 269.2–270.8°C;  $R_f$  (20% EtOAc in *n*-hexane) = 0.44;  $^1\text{H-NMR}$  (400 MHz,  $\text{DMSO-}d_6$ ):  $\delta$  7.82 (d,  $J = 8.7$  Hz, 2H, ArH), 7.62 (d,  $J = 8.7$  Hz, 2H, ArH), 6.96 (s, 1H, CH of thiazole), 6.77 (d,  $J = 8.1$  Hz, 2H), 2.11 (d,  $J = 2.0$  Hz, 2H,  $-\text{NH}_2$ );  $^{13}\text{C-NMR}$  (100 MHz,  $\text{DMSO-}d_6$ ):  $\delta$  169.1, 148.2, 146.3, 141.1, 126.7, 124.4, 107.1.

2-(2-Aminothiazol-4-yl) phenol (12). Pale yellow solid powder; yield: 43.2%; m.p.: 138–142°C;  $R_f$  (20% EtOAc in *n*-hexane) = 0.73;  $^1\text{H-NMR}$  (400 MHz,  $\text{DMSO-}d_6$ ):  $\delta$  11.56 (s, 1H, -OH), 7.24 (d,  $J = 7.7$  Hz, 1H, ArH), 7.00 (s, 1H, CH of thiazole), 6.70 (t,  $J = 7.7$  Hz, 1H, ArH), 6.61 (d,  $J = 8.2$  Hz, 1H, ArH), 6.38 (t,  $J = 8.1$  Hz, 1H, ArH), 2.09 (d,  $J = 2.7$  Hz, 2H,  $-\text{NH}_2$ );  $^{13}\text{C-NMR}$  (100 MHz,  $\text{DMSO-}d_6$ ):  $\delta$  168.6, 155.5, 147.3, 129.3, 126.4, 119.3, 118.4, 117.1, 100.8.

**2.1.3. Synthesis of 3, 5-Diphenyl-4,5-dihydro-1H-pyrazol-1-carbaldehydes (13–15).** Chalcones 13–15 (0.04 mol), 9.72 mL hydrazine hydrate (80%, 0.2 mol), and ethanol (15 mL) mixture were heated under reflux for 10 minutes until the chalcone was entirely consumed [23]. The progress of the reaction was monitored using TLC in *n*-hexane and ethyl acetate (9:1) as the mobile phase. When the reaction was completed, the warm reaction mixture was poured into ice-cold water (50 mL), and the precipitate was filtered and rinsed with water and ethanol using suction filtration. The solid produced was recrystallized with ethanol to yield *N*-formyl pyrazoline derivatives in high purity with good yields (SI Appendix A Figure S3).

4,5-Dihydro-3-(4-nitrophenyl)-5-phenylpyrazole-1-carbaldehyde (13). Reddish solid powder; yield: 87.3%; m.p.:

130–132°C;  $R_f$  (30% EtOAc in *n*-hexane) = 0.54;  $^1\text{H-NMR}$  (400 MHz,  $\text{DMSO-}d_6$ ):  $\delta$  8.48 (s, 1H, CHO), 7.82 (d,  $J = 8.5$  Hz, 2H), 7.50 (s, 2H), 7.26 (dd,  $J = 16.9, 9.1$  Hz, 2H), 6.85 (d,  $J = 8.2$  Hz, 2H), 6.16 (d,  $J = 8.4$  Hz, 1H), 5.11 (dd,  $^3J = 11.72$  Hz,  $^3J = 4.92$  Hz, 1H,  $\text{C}_5\text{-H}_X$ ), 3.54 (dd,  $^2J = 17.47$  Hz,  $^3J = 11.60$  Hz, 1H,  $\text{C}_4\text{-H}_M$ ), 3.01 (dd,  $^2J = 17.74$  Hz,  $^3J = 4.91$  Hz, 1H,  $\text{C}_4\text{-H}_A$ );  $^{13}\text{C-NMR}$  (100 MHz,  $\text{DMSO-}d_6$ ):  $\delta$  165.9, 161.1, 155.4, 148.9, 141.7, 137.5, 128.6, 126.5, 124.8, 114.3, 59.9, 42.9.

5-(4-Bromophenyl)-4,5-dihydro-3-(4-nitrophenyl)pyrazole-1-carbaldehyde (14). Yellow solid powder; yield: 78.9%; m.p.: 202–204°C;  $R_f$  (30% EtOAc in *n*-hexane) = 0.61;  $^1\text{H-NMR}$  (400 MHz,  $\text{DMSO-}d_6$ ):  $\delta$  8.50 (s, 1H, CHO), 7.87 (dd,  $J = 8.8, 3.5$  Hz, 4H), 7.38 (d,  $J = 8.6$  Hz, 3H), 7.11 (d,  $J = 8.0$  Hz, 5H), 6.89 (d,  $J = 8.1$  Hz, 3H), 4.55 (dd,  $^3J = 11.81$  Hz,  $^3J = 5.29$  Hz, 1H,  $\text{C}_5\text{-H}_X$ ), 3.58 (dd,  $^2J = 17.27$  Hz,  $^3J = 11.71$  Hz, 1H,  $\text{C}_4\text{-H}_M$ ), 3.10 (dd,  $^2J = 17.24$  Hz,  $^3J = 4.81$  Hz, 1H,  $\text{C}_4\text{-H}_A$ );  $^{13}\text{C-NMR}$  (100 MHz,  $\text{DMSO-}d_6$ ):  $\delta$  166.5, 160.3, 155.9, 146.2, 141.9, 131.3, 128.8, 125.9, 123.9, 120.3, 63.3, 48.6.

4,5-Dihydro-5-(2-hydroxyphenyl)-3-(4-nitrophenyl)pyrazole-1-carbaldehyde (15). Pale yellow solid powder; yield: 92.5%; m.p.: 175–177°C;  $R_f$  (30% EtOAc in *n*-hexane) = 0.79;  $^1\text{H-NMR}$  (400 MHz,  $\text{DMSO-}d_6$ ):  $\delta$  10.65 (s, 1H), 8.55 (s, 1H, CHO), 7.58 (d,  $J = 8.2$  Hz, 2H), 7.25 (d,  $J = 7.7$  Hz, 2H), 7.00 (d,  $J = 7.6$  Hz, 2H), 5.81 (dd,  $^3J = 11.71$  Hz,  $^3J = 4.94$  Hz, 1H,  $\text{C}_5\text{-H}_X$ ), 2.76 (dd,  $^2J = 17.27$  Hz,  $^3J = 11.71$  Hz, 1H,  $\text{C}_4\text{-H}_M$ ), 2.10 (dd,  $^2J = 17.14$  Hz,  $^3J = 5.29$  Hz, 1H,  $\text{C}_4\text{-H}_A$ );  $^{13}\text{C-NMR}$  (100 MHz,  $\text{DMSO-}d_6$ ):  $\delta$  167.3, 163.7, 159.4, 148.5, 134.2, 131.8, 128.0, 124.5, 124.4, 124.3, 120.5, 118.8, 79.78, 49.4.

**2.1.4. Synthesis of Thiazolyl-Pyrazoline Schiff Base Hybrids in the Presence of ZnO Nanoparticles as a Catalyst Derived from Chalcones (16–24).** The target Schiff base hybrids were synthesized by condensation of an equimolar ethanolic solution (20 mL) of *N*-formyl pyrazoline derivatives, 13–15 (3 mmol), with substituted 2-amino-4-(substituted-phenyl)

thiazole derivatives, 10–12 (3 mmol equiv.), in ZnO nanoparticles (43 mg, 0.2 mmol, 20 mol %) as a catalyst in methanol (20 mL) under reflux for 3 h. The progress of the reaction was monitored using TLC at an appropriate time interval using *n*-hexane: ethyl acetate (7 : 3). At the end of the reaction, the solution was slowly evaporated, and the precipitate was filtered, washed with ethanol, and dried under a vacuum. Finally, the resulting solid was recrystallized from ethanol to provide a microcrystalline solid product (Scheme 3 and SI Appendix A Figure S4).

(18E)-N-((4,5-dihydro-3-(4-nitrophenyl)-5-phenylpyrazol-1-yl)methylene)-4-phenylthiazol-2-amine (16). Reddish yellow solid powder; yield: 94.7%; m.p.: 258–260 °C; Mol. wt = 453.52; chemical formula: C<sub>25</sub>H<sub>19</sub>N<sub>5</sub>O<sub>2</sub>S; R<sub>f</sub> (20% EtOAc in *n*-hexane) = 0.17; UV-visible (MeOH) λ<sub>max</sub> = 285 and 385 nm; <sup>1</sup>H-NMR (400 MHz, DMSO-*d*<sub>6</sub>): δ 8.49 (s, 1H, CH =N), 7.94–7.81 (m, 1H), 7.78 (s, 1H, Ar-H of thiazole-H), 7.56 (d, *J* = 8.5 Hz, 2H), 7.37 (d, *J* = 8.5 Hz, 2H), 7.10 (d, *J* = 8.3 Hz, 2H), 6.89 (d, *J* = 8.0 Hz, 2H), 6.78 (d, *J* = 8.0 Hz, 1H), 6.73 (d, *J* = 8.4 Hz, 1H), 5.13 (d, *J* = 6.8 Hz, 2H), 4.55 (dd, <sup>3</sup>*J* = 11.82, <sup>3</sup>*J* = 6.24 Hz, 1H, C<sub>5</sub>-H<sub>X</sub>), 3.12 (dd, <sup>2</sup>*J* = 17.77, <sup>3</sup>*J* = 11.82 Hz, 1H, C<sub>4</sub>-H<sub>M</sub>), 2.48 (dd, <sup>2</sup>*J* = 17.84, <sup>3</sup>*J* = 4.62 Hz, 1H, C<sub>4</sub>-H<sub>A</sub>); <sup>13</sup>C-NMR (100 MHz, DMSO-*d*<sub>6</sub>): δ 160.7, 156.4, 155.1, 153.1, 148.4, 146.6, 142.3, 139.8, 137.4, 131.9, 129.2, 128.6, 128.2, 126.4, 124.4, 121.1, 120.75, 63.7, 49.0.

(18E)-N-((4,5-dihydro-3-(4-nitrophenyl)-5-phenylpyrazol-1-yl)methylene)-4-(4-nitrophenyl)thiazol-2-amine (17). Orange solid powder; yield: 90.7%; m.p.: 255–257 °C; R<sub>f</sub> (20% EtOAc in *n*-hexane) = 0.27; UV-visible (MeOH) λ<sub>max</sub> = 285 and 340 nm; <sup>1</sup>H-NMR (400 MHz, DMSO-*d*<sub>6</sub>): δ 8.50 (s, 1H, CH =N), 7.85 (d, *J* = 8.2 Hz, 2H), 7.78 (d, *J* = 8.4 Hz, 2H), 7.59 (d, *J* = 8.5 Hz, 1H), 7.38 (s, 1H, Ar-H of thiazole-H), 6.92 (d, *J* = 8.2 Hz, 2H), 6.85–6.74 (m, 1H), 6.74 (d, *J* = 8.1 Hz, 2H), 6.18 (d, *J* = 8.3 Hz, 1H), 5.15 (dd, <sup>3</sup>*J* = 11.12, <sup>3</sup>*J* = 5.74 Hz, 1H, C<sub>5</sub>-H<sub>X</sub>), 4.50 (dd, <sup>2</sup>*J* = 18.21, <sup>3</sup>*J* = 12.21 Hz, 1H, C<sub>4</sub>-H<sub>M</sub>), 3.57 (dd, <sup>2</sup>*J* = 17.44, <sup>3</sup>*J* = 5.19 Hz, 1H, C<sub>4</sub>-H<sub>A</sub>); <sup>13</sup>C-NMR (100 MHz, DMSO-*d*<sub>6</sub>): δ 169.1, 160.7, 159.5, 157.2, 155.0, 151.6, 148.5, 146.3, 137.1, 129.2, 126.7, 124.4, 124.3, 118.0, 113.9, 107.1, 59.3, 42.7.

2-((2E)-2-((4,5-dihydro-3-(4-nitrophenyl)-5-phenylpyrazol-1-yl)methyleneamino)thiazol-4-yl)phenol (18). Orange solid powder; yield: 90.2%; m.p.: 198–200 °C; R<sub>f</sub> (20% EtOAc in *n*-hexane) = 0.39; UV-visible (MeOH) λ<sub>max</sub> = 285 and 390 nm; <sup>1</sup>H-NMR (400 MHz, DMSO-*d*<sub>6</sub>): δ 11.18 (s, OH), 8.47 (s, 1H, CH =N), 7.81 (d, *J* = 8.3 Hz, 2H), 7.75 (s, 1H, Ar-H of thiazole-H), 7.52 (d, *J* = 8.4 Hz, 2H), 7.21 (d, *J* = 7.9 Hz, 2H), 6.98 (d, *J* = 8.2 Hz, 2H), 6.89 (t, *J* = 7.6 Hz, 1H), 6.77 (d, *J* = 7.6 Hz, 2H), 6.57 (d, *J* = 8.0 Hz, 1H), 6.36 (d, *J* = 8.2 Hz, 2H), 6.17 (t, *J* = 8.8 Hz, 1H), 5.11 (dd, <sup>3</sup>*J* = 11.62, <sup>3</sup>*J* = 4.95 Hz, 1H, C<sub>5</sub>-H<sub>X</sub>), 4.53 (dd, <sup>2</sup>*J* = 17.91, <sup>3</sup>*J* = 11.23 Hz, 1H, C<sub>4</sub>-H<sub>M</sub>), 3.53 (dd, <sup>2</sup>*J* = 18.43, <sup>3</sup>*J* = 6.23 Hz, 1H, C<sub>4</sub>-H<sub>A</sub>); <sup>13</sup>C-NMR (100 MHz, DMSO-*d*<sub>6</sub>): δ 168.8, 160.6, 155.7, 155.0, 151.6, 148.5, 147.5, 142.8, 141.2, 137.1, 129.5, 128.2, 128.1, 126.62, 126.1, 124.2, 119.4, 117.3, 113.9, 59.5, 42.5.

(18E)-N-((5-(4-bromophenyl)-4,5-dihydro-3-(4-nitrophenyl)pyrazol-1-yl)methylene)-4-phenylthiazol-2-amine (19). Yellow solid powder; yield: 92.6%; m.p.: 251–253 °C; R<sub>f</sub> (20% EtOAc in *n*-hexane) = 0.70; UV-visible (MeOH) λ<sub>max</sub> = 285 and 390 nm; <sup>1</sup>H-NMR (400 MHz, DMSO-*d*<sub>6</sub>): δ

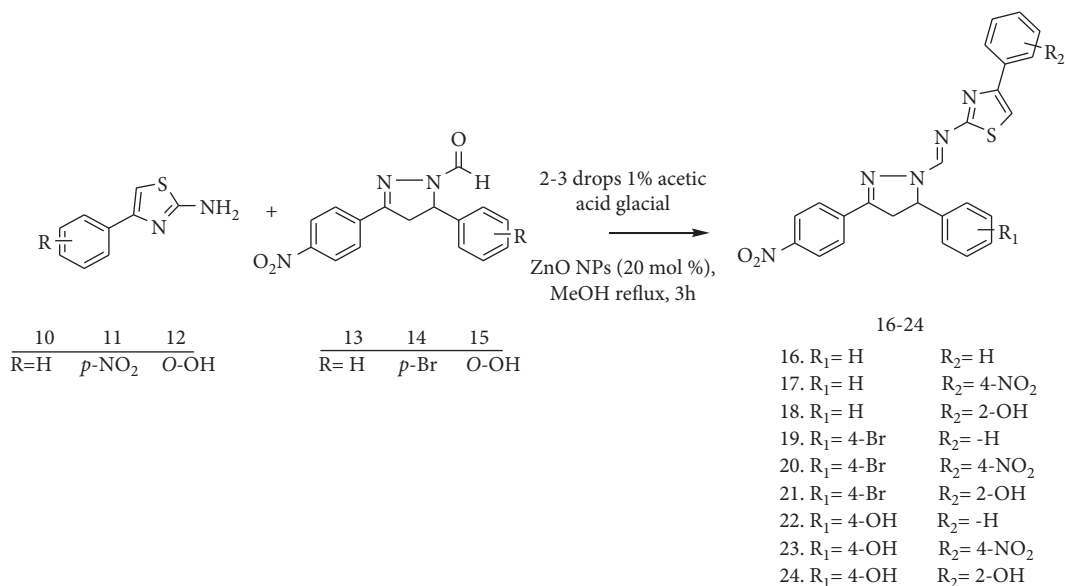
8.44 (s, 1H, CH =N), 7.78 (d, *J* = 8.4 Hz, 2H), 7.71 (d, *J* = 11.8 Hz, 1H), 7.50 (d, *J* = 8.4 Hz, 1H), 7.29 (d, *J* = 8.2 Hz, 1H), 7.25 (d, *J* = 8.7 Hz, 1H), 6.97 (d, *J* = 8.4 Hz, 1H), 6.96–6.54 (m, 5H), 6.51 (s, 1H, Ar-H of thiazole-H), 6.42 (d, *J* = 6.5 Hz, 1H), 6.14 (d, *J* = 8.2 Hz, 1H), 5.10 (dd, <sup>3</sup>*J* = 12.82, <sup>3</sup>*J* = 6.85 Hz, 1H, C<sub>5</sub>-H<sub>X</sub>), 4.47 (dd, <sup>2</sup>*J* = 18.22, <sup>3</sup>*J* = 12.13 Hz, 1H, C<sub>4</sub>-H<sub>M</sub>), 3.50 (dd, <sup>2</sup>*J* = 18.43, <sup>3</sup>*J* = 6.23 Hz, 1H, C<sub>4</sub>-H<sub>A</sub>); <sup>13</sup>C-NMR (100 MHz, DMSO-*d*<sub>6</sub>): δ 169.1, 160.6, 155.0, 148.5, 141.6, 137.1, 134.1, 129.5, 128.4, 125.9, 124.3, 118.2, 114.0, 102.2, 59.5, 42.5.

(18E)-N-((5-(4-bromophenyl)-4,5-dihydro-3-(4-nitrophenyl)pyrazol-1-yl)methylene)-4-(4-nitrophenyl)thiazol-2-amine (20). Yellow solid powder; yield: 89.8%; m.p.: 247–249 °C; R<sub>f</sub> (20% EtOAc in *n*-hexane) = 0.71; UV-visible (MeOH) λ<sub>max</sub> = 285 and 380 nm; <sup>1</sup>H-NMR (400 MHz, DMSO-*d*<sub>6</sub>): δ 8.49 (s, 1H, CH =N), 7.92 (dd, *J* = 11.4, 7.0 Hz, 1H), 7.89–7.62 (m, 1H), 7.57 (dd, *J* = 11.4, 7.0 Hz, 2H), 7.36 (d, *J* = 9.4 Hz, 1H), 7.10 (d, *J* = 9.6 Hz, 1H), 6.92 (s, 1H, Ar-H of thiazole-H), 6.78 (d, *J* = 8.3 Hz, 1H), 5.54 (dd, <sup>3</sup>*J* = 11.13, <sup>3</sup>*J* = 5.95 Hz, 1H, C<sub>5</sub>-H<sub>X</sub>), 3.52 (dd, <sup>2</sup>*J* = 17.49, <sup>3</sup>*J* = 4.99 Hz, 1H, C<sub>4</sub>-H<sub>M</sub>), 2.89 (dd, <sup>2</sup>*J* = 18.73, <sup>3</sup>*J* = 6.44 Hz, 1H, C<sub>4</sub>-H<sub>A</sub>); <sup>13</sup>C-NMR (100 MHz, DMSO-*d*<sub>6</sub>): δ 169.1, 160.7, 156.4, 155.0, 153.0, 148.2, 146.3, 143.7, 141.1, 132.4, 129.9, 128.6, 127.6, 126.7, 124.6, 121.1, 107.1, 59.9, 48.5.

2-((2E)-2-((5-(4-bromophenyl)-4,5-dihydro-3-(4-nitrophenyl)pyrazol-1-yl)methyleneamino)thiazol-4-yl)phenol (21). Pale yellow solid powder; yield: 78.3%; m.p.: 258–260 °C; R<sub>f</sub> (20% EtOAc in *n*-hexane) = 0.26; UV-visible (MeOH) λ<sub>max</sub> = 285 and 395 nm; <sup>1</sup>H-NMR (400 MHz, DMSO-*d*<sub>6</sub>): δ 10.19 (s, OH), 8.49 (s, 1H, CH =N), 7.92–7.80 (m, 2H), 7.76 (d, *J* = 8.2 Hz, 1H), 7.70 (d, *J* = 8.5 Hz, 1H), 7.56 (dd, *J* = 11.9, 8.3 Hz, 2H), 7.23 (d, *J* = 7.8 Hz, 1H), 7.09 (d, *J* = 7.8 Hz, 3H), 6.75 (dd, *J* = 10.9, 8.1 Hz, 2H), 6.60 (s, 1H, Ar-H of thiazole-H), 6.38 (d, *J* = 8.5 Hz, 2H), 5.12 (dd, *J* = 12.0, 5.5 Hz, 1H), 4.51 (dd, <sup>3</sup>*J* = 11.79, <sup>3</sup>*J* = 4.94 Hz, 1H, C<sub>5</sub>-H<sub>X</sub>), 3.33 (dd, <sup>2</sup>*J* = 17.18, <sup>3</sup>*J* = 5.22 Hz, 1H, C<sub>4</sub>-H<sub>M</sub>), 3.06 (dd, <sup>2</sup>*J* = 17.73, <sup>3</sup>*J* = 5.47 Hz, 1H, C<sub>4</sub>-H<sub>A</sub>); <sup>13</sup>C-NMR (100 MHz, DMSO-*d*<sub>6</sub>): δ 169.1, 160.7, 156.4, 146.7, 142.3, 140.6, 139.8, 139.3, 137.0, 131.8, 129.2, 126.6, 126.4, 124.4, 124.0, 119.4, 118.5, 117.3, 107.0, 101.0, 63.7, 43.8.

2-(1-((E)-(4-phenylthiazol-2-ylimino)methyl)-4,5-dihydro-3-(4-nitrophenyl)-1H-pyrazol-5-yl)phenol (22). Yellow solid powder; yield: 86.3%; m.p.: 248–250 °C; R<sub>f</sub> (20% EtOAc in *n*-hexane) = 0.51; UV-visible (MeOH) λ<sub>max</sub> = 285 and 395 nm; <sup>1</sup>H-NMR (400 MHz, DMSO-*d*<sub>6</sub>): δ 10.79 (s, OH), 8.56 (s, 1H, CH =N), 8.41 (d, *J* = 14.3 Hz, 1H), 7.90 (d, *J* = 8.5 Hz, 2H), 7.81 (s, 1H, Ar-H of thiazole-H), 7.86–7.69 (m, 2H), 7.62 (dd, *J* = 16.8, 8.7 Hz, 1H), 7.36–7.23 (m, 2H), 7.05–6.95 (m, 2H), 5.01 (dd, <sup>3</sup>*J* = 12.33, <sup>3</sup>*J* = 6.12 Hz, 1H, C<sub>5</sub>-H<sub>X</sub>), 3.96 (dd, <sup>2</sup>*J* = 17.41, <sup>3</sup>*J* = 5.79 Hz, 1H, C<sub>4</sub>-H<sub>M</sub>), 3.55 (dd, <sup>2</sup>*J* = 17.72, <sup>3</sup>*J* = 4.92 Hz, 1H, C<sub>4</sub>-H<sub>A</sub>); <sup>13</sup>C-NMR (100 MHz, DMSO-*d*<sub>6</sub>): δ 175.1, 166.3, 163.4, 162.7, 158.4, 155.8, 148.1, 147.8, 143.1, 133.1, 130.8, 128.0, 127.6, 127.0, 123.4, 123.4, 119.5, 118.2, 116.3, 75.6, 48.4.

2-(1-((E)-(4-(4-nitrophenyl)thiazol-2-ylimino)methyl)-4,5-dihydro-3-(4-nitrophenyl)-1H-pyrazol-5-yl)phenol (23). Yellow solid powder; yield: 91.6%; m.p.: 200–220 °C; R<sub>f</sub> (20% EtOAc in *n*-hexane) = 0.56; UV-visible (MeOH) λ<sub>max</sub> = 285 and 385 nm; <sup>1</sup>H-NMR (400 MHz, DMSO-*d*<sub>6</sub>): δ 10.79 (s,



SCHEME 3: Synthesis of thiazolyl-pyrazoline Schiff base hybrids derived from chalcone (16–24).

OH), 8.54 (s, 1H, CH =N), 7.88 (d,  $J=8.7$  Hz, 1H), 7.80 (d,  $J=8.6$  Hz, 2H), 7.60 (d,  $J=8.6$  Hz, 2H), 7.33–7.22 (m, 1H), 6.99 (d,  $J=7.0$  Hz, 1H), 6.75 (s, 1H, Ar-H of thiazole-H), 6.56 (d,  $J=4.7$  Hz, 1H), 5.17 (dd,  $^3J=11.35$ ,  $^3J=4.59$  Hz, 1H,  $C_5\text{-H}_X$ ), 3.94 (dd,  $^2J=17.49$ ,  $^3J=4.59$  Hz, 1H,  $C_4\text{-H}_M$ ), 3.25 (dd,  $^2J=17.92$ ,  $^3J=4.92$  Hz, 1H,  $C_4\text{-H}_A$ );  $^{13}\text{C-NMR}$  (100 MHz,  $\text{DMSO-}d_6$ ): $\delta$  169.1, 163.3, 161.8, 158.9, 156.4, 148.7, 146.3, 143.7, 141.1, 133.8, 131.5, 128.6, 126.7, 124.4, 124.0, 120.1, 118.4, 116.9, 107.1, 66.3, 49.0.

2-(1-((E)-(2-thiazol-4-yl)phenol)methyl)-4,5-dihydro-3-(4-nitrophenyl)-1H-pyrazol-5-yl)phenol (24). Bright yellow solid powder; yield; 92.9%; m.p.: 220–222°C;  $R_f$  (20% EtOAc in *n*-hexane) = 0.72; UV-visible (MeOH)  $\lambda_{\text{max}}=285$  and 395 nm;  $^1\text{H-NMR}$  (400 MHz,  $\text{DMSO-}d_6$ ): $\delta$  10.89 (s, OH), 10.77 (s, OH), 8.52 (s, 1H, CH =N), 8.38 (s, 1H, Ar-H of thiazole-H), 7.85 (d,  $J=9.0$  Hz, 4H), 7.83–7.76 (m, 1H), 7.80–7.63 (m, 5H), 7.33–7.18 (m, 5H), 7.02–6.93 (m, 5H), 6.84–6.61 (m, 1H), 6.59 (d,  $J=17.0$  Hz, 2H), 6.55–6.45 (m, 2H), 6.38 (d,  $J=7.9$  Hz, 2H), 6.20 (s, 1H, Ar-H of thiazole-H), 5.57 (dd,  $^3J=11.95$ ,  $^3J=5.22$  Hz, 1H,  $C_5\text{-H}_X$ ), 3.94 (dd,  $^2J=17.51$ ,  $^3J=5.29$  Hz, 1H,  $C_4\text{-H}_M$ ), 3.88 (dd,  $^2J=17.52$ ,  $^3J=5.22$  Hz, 1H,  $C_4\text{-H}_A$ );  $^{13}\text{C-NMR}$  (100 MHz,  $\text{DMSO-}d_6$ ): $\delta$  168.8, 163.9, 163.3, 159.1, 156.4, 155.7, 148.7, 148.4, 147.5, 143.6, 133.7, 131.4, 128.2, 127.7, 126.6, 124.0, 120.1, 120.1, 118.4, 116.8, 101.1, 49.0, 40.1.

## 2.2. Biological Activity Evaluations

**2.2.1. In Vitro Antibacterial Activity.** The antibacterial susceptibility of each bacterial strain to all synthesized compounds was assessed using the Clinical and Laboratory Standards Institute (CLSI) procedures using agar disc diffusion assay. The inhibition zone technique shows the ability of a compound or drug to prevent microbial growth [24]. The Adama Public Health Research and Referral Laboratory Center provided four strains of pathogenic microorganisms

of two Gram-positive bacteria, including the MRSA strain of *Staphylococcus aureus* (ATCC 25923) and *Streptococcus pyogenes* (ATCC 27853), and two Gram-negative bacteria, *Escherichia coli* (ATCC 25922) and *Pseudomonas aeruginosa* (ATCC 27853). Colony morphology and Gram staining, as well as routine biochemical assays, were used to identify and authenticate the bacterial strains, according to Bergey's Manual of Determinative Bacteriology [25]. The antibacterial activity was assessed at 250 and 500  $\mu\text{g/mL}$  concentrations by measuring the zone of inhibition against the test organisms and comparing it with amoxicillin as the reference antibiotic. Amoxicillin (25 and 50 mg/mL) was the standard drug used as a positive control, and DMSO was used as a negative control. The experiments were repeated three times, and the average clear zone (inhibition zone) around each compound was measured in millimeters (mm) [26].

**2.2.2. DPPH Free Radical Scavenging Assay.** By bleaching the purple color of a methanolic solution of DPPH, the ability of the related compounds to transfer hydrogen atoms or electrons was measured. The 2,2-diphenyl-1-picrylhydrazyl (DPPH) approach was used to examine the *in vitro* radical scavenging activity of the synthesized compounds with minor adjustments [27]. To a solution of 1 ml of 0.004% methanolic solution of diphenyl picrylhydrazyl (DPPH), 4 ml of various sample concentrations was added. After 60 minutes in the dark, the absorbance was measured against a blank at 517 nm using a double-beam UV-vis spectrophotometer. The blank reading solution was methanol, while the standard solution was ascorbic acid, which was calculated by the following equation:

$$\% \text{ DPPH free radical scavenging} = \frac{A_{\text{blank}} - A_{\text{sample}}}{A_{\text{blank}}} \times 100, \quad (1)$$

where  $A_{\text{control}}$  = the absorbance of the control (DPPH without compound) and  $A_{\text{sample}}$  = the absorbance of the test sample. To determine the  $IC_{50}$ , different concentrations of the test compounds in methanol (12.5 to 200 g/mL) were added to a methanolic solution of DPPH (the concentration that makes 50% inhibition of the DPPH color). All  $IC_{50}$  values were computed from the corresponding sigmoidal dose-response curve according to their best-fit shapes based on at least five reaction points using the Office Excel 2007 software (Microsoft, Redmond, WA, USA). All experiments were carried out in triplicates to calculate the mean and standard deviation statistically.

**2.2.3. In Vitro Lipid Peroxidation Inhibition Assay.** Lipid peroxidation proceeds in the form of a self-sustaining chain reaction and is very harmful. The formation of lipid-free radicals and lipid peroxide radicals in the cell membranes is considered an important feature of the cell damage caused by reactive oxygen species [28]. Ascorbic acid was used as a positive control. The percentage of lipid peroxidation inhibition was calculated from the following equation:

$$\% \text{ lipid peroxidation inhibition} = \frac{A_{\text{control}} - A_{\text{compound}}}{A_{\text{compound}}} \times 100, \quad (2)$$

where  $A_{\text{sample}}$  = absorbance of the sample and  $A_{\text{control}}$  = absorbance of control. The percentage of lipid peroxidation inhibition was plotted against the synthetic compound concentration to determine the concentration required to achieve 50% inhibition of phospholipid oxidation ( $IC_{50}$ ) in linoleic acid; ascorbic acid was used as a positive control.

#### 2.2.4. In Silico Computational Studies

**(1) ADMET, Drug-Likeness, and Toxicity Prediction.** The prediction of the *in silico* ADMET parameters before the experimental studies is one of the most important aspects of drug discovery and development processes. ADMET studies play a critical role in helping to optimize the pharmacokinetic and pharmacodynamic properties of new drugs [29]. This prediction is based on an already established concept by the Lipinski rule of five [30] and the Veber rule [31]. Properties of the compounds were estimated using ADME descriptors by using SwissADME (<https://www.swissadme.ch/>), Molinspiration (<https://www.molinspiration.com/>), and PreADMET (<https://preadmet.webservice.bmdrc.org/>) online servers. Structures of compounds were submitted to SwissADME tools and converted to their canonical simplified molecular-input line-entry system (SMILES), to estimate *in silico* pharmacokinetic parameters and other molecular properties based on the reported method [32]. The organ toxicity profiles and toxicological endpoints of the ligands and toxicity class were predicted using ProTox-II Web server explorer (<https://tox-new.charite.de/>).

**2.2.5. Molecular Docking Study.** A molecular docking study was performed to investigate the binding mode between the synthesized compounds against target enzymes. ChemDraw program (Chem Create 16.0) was used to draw chemical structures of compounds with suitable 2D orientation, and ChemDraw Ultra 8.0 was employed to minimize the energy of ligands and standard drugs. The protein preparation and docking simulation were then carried out using the energy-minimized ligand molecules as input to AutoDock Vina 4.2.6 [33]. The DNA gyrase B (PDB ID: 6f86), the N-terminal domain of PqsA in complex with 6-fluoroanthraniloyl-AMP (PDB ID:5oe3), Pyruvate Kinase in complex with bis-indole alkaloid (PDB ID:3t07), LuxS of *S. pyogenes* (Uniprot id: P0C0C7), and Human peroxiredoxin 5 (PDB ID: 1HD2) crystal structures were downloaded from the Protein Data Bank (<https://www.rcsb.org>) to investigate the binding interaction of the synthesized compounds with the active site of protein targets using the following grid box parameters (PDB ID: 6f86) [62 × 30 × 64], [15 × 14 × 19], (PDB ID:5oe3) [38 × 2 × 17], [19 × 21 × 14], (PDB ID:3t07) [−15 × −3 × 2], [18 × 14 × 16], (Uniprot id: P0C0C7) [46 × 45 × 39], [14 × 12 × 17], and (PDB ID:1HD2) [6 × 44 × 33], [15 × 18 × 17], respectively [34]. The best-docked conformation between ligand and protein was searched using the docking algorithm with AutoDock Vina. During the docking process, a maximum of nine conformers were considered for each ligand. Meanwhile, the Discovery Studio Visualizer 2021 and PyMOL (version 2.4) were used to investigate the possible interactions and ligand orientations between the target receptor and ligands by identifying conformations to optimize the docking function [35].

### 3. Results and Discussion

A series of novel thiazolyl-pyrazoline Schiff base hybrids were synthesized and characterized using spectroscopic methods with good to excellent yields (78.3–96.9%). Shorter reaction times were achieved for the ZnO nanoparticle-catalyzed approach compared with the conventional glacial acetic acid-catalyzed reactions under reflux conditions. Physical properties and NMR spectral data of the synthesized compounds are presented in supporting information (SI Appendix B Figures 19–45).

**3.1. Recyclability Study of the Catalyst.** A good catalyst for scale-up applications should have high activity and stability. After the reaction was completed, the catalyst was filtered, washed with dichloromethane and methanol, and dried at 100°C for 5 hr before being used in the next cycle with no apparent loss of activity, making this technique cost-effective and environmentally benign (SI Appendix A, Table S3) [36]. The catalyst ZnO NPs were found to have good catalytic activity for six consecutive runs with no appreciable catalytic activity loss and delivered a modest decrease in reaction yield (Figure 1). ZnO nanoparticle catalysis provides a shorter time and a higher product yield compared with typical acid catalysts [37, 38].

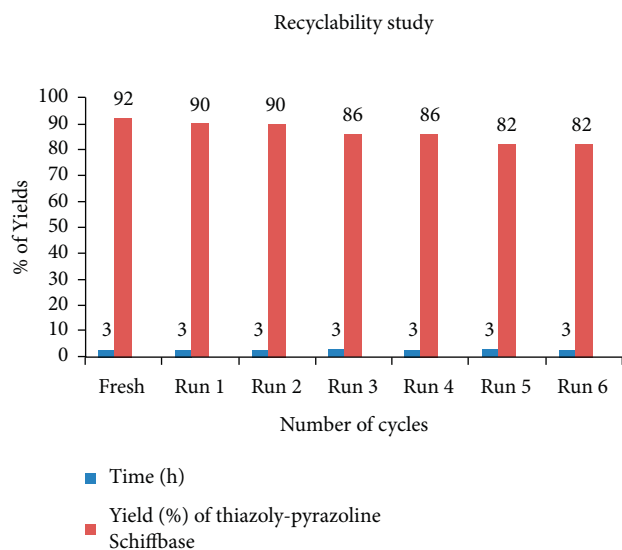


FIGURE 1: Synthesis of thiazolyl-pyrazoline Schiff base hybrids from chalcone catalyzed by ZnO NPs was investigated for recyclability.

### 3.2. General Synthesis

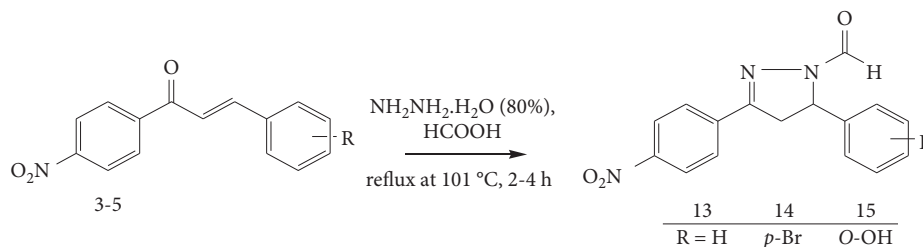
**3.2.1. General Synthesis of Chalcone Derivatives (3–5).** Chalcone scaffolds were synthesized at room temperature by combining *p*-nitro acetophenone with various substituted aryl aldehydes via a basic catalyzed Claisen–Schmidt condensation reaction (Scheme 1 and SI Appendix A Figure S1). The aryl ring substitution pattern was carefully chosen to provide a variety of electronic environments that would affect the target molecules' antibacterial and antioxidant activity patterns. In the  $^1\text{H-NMR}$  spectrum of compounds (3–5),  $\text{H-}\beta$  and  $\text{H-}\alpha$  protons of  $\alpha$ ,  $\beta$ -conjugated system of chalcone appeared as a broad doublet in between  $\delta$  7.75–7.73 and  $\delta$  7.32–7.39, respectively, with a coupling constant of  $^3J = 15.6\text{ Hz}$ , which agrees with a trans-configuration. For compound 3, AAXX' spin system aromatic protons for ring A and monosubstituted ring B are evident at  $\delta$  7.43–7.95. For compound 4, two sets of AAXX' spin system aromatic protons are observed between  $\delta$  7.23–7.46 and  $\delta$  7.52–7.96. For compound 5, AAXX' spin system aromatic protons for ring A and disubstituted ring B are evident at  $\delta$  7.70–7.88 and  $\delta$  8.00–8.04, respectively. In the  $^{13}\text{C-NMR}$  spectrum of compounds (3–5), the C- $\beta$  and C- $\alpha$  signals appeared at  $\delta$  138.4 and 120.1, respectively, while the carbonyl group appeared between  $\delta$  167 and 189.9.

**3.2.2. General Synthesis of 2-Amino-4-(substituted-phenyl)thiazole Derivatives (10–12).** Thiazole amine derivatives 10–12 were synthesized (Scheme 2, SI Appendix A Figure S2) by reacting substituted acetophenone and thio-urea in the presence of a catalyst, and the intermediate 4-(4-substituted-phenyl)thiazol-2-amines (10–12) were obtained from good to excellent yields in a single Step (48.2–96.6%). The singlet at  $\delta$  2.9 in the  $^1\text{H-NMR}$  spectrum of 10–12 confirms the existence of the  $-\text{NH}_2$  group. The singlet at  $\delta$  6.9–7.80 suggests the presence of  $\text{sp}^2$  methine in the thiazole ring. Aromatic methine peaks were observed between  $\delta$  6.93

and 7.52. The proposed thiazole derivative molecular structures are in good agreement with the  $^{13}\text{C-NMR}$  spectrum, i.e., phenyl ring peaks at  $\delta$  119.2, 127.6, 128.4, 131.2, and 143.3, and peaks that belong to thiazole ring appeared at  $\delta$  107.4, 148.2, and 165.1.

**3.2.3. General Synthesis of N-Formyl Pyrazoline Derivatives (13–15).** Chalcones (3–5) were used as the starting material for a nucleophilic cycloaddition reaction with hydrazine hydrate to form intermediates of N-formyl pyrazolines (13–15). The N-formyl pyrazoline ring is produced by cyclization and dehydration of chalcone derivatives after a 1,4-Michael addition of hydrazine. The synthesis of N-formyl pyrazoline derivatives (13–15) was found to be in good to excellent yields (80–96%) in two steps (Scheme 4 and SI Appendix A Figure S3). In the  $^1\text{H-NMR}$  spectrum, the diastereotopic protons  $H_A$ ,  $H_M$ , and  $H_X$  that correspond to the pyrazoline nucleus display an AMX spin pattern where  $H_A$  and  $H_M$  each appear as a doublet of a doublet at  $H_A$  appeared at  $\delta$  2.91–3.06 (dd,  $^2J_{AM} = 17.41\text{--}17.87$ ,  $^3J_{AX} = 4.91\text{--}6.87\text{ Hz}$ , C<sub>4</sub>-H<sub>X</sub> of pyrazoline) and  $H_M$  at  $\delta$  3.42–3.90 (dd,  $^2J_{MA} = 17.27\text{--}17.47\text{ Hz}$ ,  $^3J_{MX} = 11.60\text{--}11.71\text{ Hz}$ , C<sub>4</sub>'-H<sub>X</sub> of pyrazoline). The  $H_X$  methine (C-H) proton of pyrazoline moiety appeared in the range of  $\delta$  4.60–5.65 with coupling constants of (dd,  $^3J_{AX} = 11.71\text{--}11.81$ ,  $^3J_{MX} = 4.92\text{--}5.29\text{ Hz}$ , C<sub>5</sub>-H<sub>X</sub> of pyrazoline) suggesting vicinal coupling of methine with magnetically nonequivalent methylene protons. The aldehyde proton signal appeared as a singlet at  $\delta$  8.93–9.23. The  $^{13}\text{C-NMR}$  spectrum shows that the methylene carbon,  $\text{sp}^3$  methine, and  $\text{sp}^2$  quaternary carbons of the pyrazoline ring appeared C-4 at  $\delta$  42.2–44.09, C-5 at  $\delta$  62.7–65.02, and C-3 at  $\delta$  155.8, respectively, whereas the aldehyde carbonyl carbon appeared in between at  $\delta$  160.1 and 167.5 range confirming the formation of N-formyl pyrazoline derivatives (13–15). All the other aromatic were observed in the expected regions.

**3.2.4. General Synthesis of Thiazolyl-Pyrazoline Schiff Base Hybrids (16–24).** A series of novel thiazolyl-pyrazoline Schiff base hybrids were synthesized via a Schiff base reaction between 2-amino-4-(substituted-phenyl)thiazole (10–12) and N-formyl-3,5-diphenyl-4,5-dihydro-(1H)-pyrazole derivatives (13–15) in the presence of ZnO nanoparticles as a heterogeneous catalyst in ethanol reflux (Scheme 3). The scope of the optimized method was checked with electron-donating and electron-withdrawing substituents at phenyl rings.  $^1\text{H-NMR}$  spectra of target products (16–24) revealed three doublets of doublets as an AMX spin pattern with varying coupling constant ( $J$ ) values, two diastereotopic methylene protons of  $H_A$  and  $H_M$ , and  $\text{sp}^3$  methine proton  $H_X$  of pyrazoline nucleus. Protons  $H_A$  and  $H_B$  appeared as two doublets of a doublet in the range of  $\delta$  3.09–3.35 (dd,  $J_{AM} = 17.2\text{--}17.85\text{ Hz}$ ,  $J_{AX} = 4.78\text{--}6.88\text{ Hz}$ , C<sub>4</sub>-H<sub>A</sub>) and  $\delta$  3.42–3.90 (dd,  $J_{MA} = 17.60\text{--}17.97\text{ Hz}$ ,  $J_{MX} = 11.20\text{--}11.88\text{ Hz}$ , C<sub>4</sub>'-H<sub>M</sub>) due to vicinal and geminal coupling, respectively. Proton  $H_X$  exhibited a signal having doublet of doublet in the region  $\delta$  4.60–5.64 with  $J_{XA} = 11.38\text{--}11.87\text{ Hz}$ ,  $J_{MX} = 4.92\text{--}6.80\text{ Hz}$ , C<sub>5</sub>-H<sub>X</sub> due to vicinal coupling with two



SCHEME 4: Synthesis of (N)-formyl pyrazoline derivatives (13–15).

nonequivalent methylene protons of pyrazoline nucleus. A signal having singlet seen at  $\delta$  7.00–8.68 attributed to  $sp^2$  methine proton of thiazole ring. The azomethine  $sp^2$  methine proton (CH=N) was also detected as a singlet at  $\delta$  9.19. In addition, all the other aromatic protons were found in the expected regions. The  $^{13}C$ -NMR spectrum of the compounds (16–24) showed peaks at  $\delta$  151.1 attributed to  $sp^2$  methine of azomethine group (-CH=N) ring, respectively. The signals at  $\delta$  164.8–165.1, 148.6–152.3, and 102.8–109.5 attributed to  $sp^2$  quaternary carbons of thiazole ring rings. Moreover,  $sp^2$  quaternary carbon,  $sp^3$  methine, and methylene carbons of the pyrazoline moiety were observed around  $\delta$  152.4–153.8,  $\delta$  63.2–64.7, and  $\delta$  43.4–43.9, respectively. Furthermore, aromatic ring  $sp^2$  methines and  $sp^2$  quaternary carbons appeared within expected ranges of  $\delta$  117.4–164.1 (16–24, SI Appendix A Figure S4). A plausible mechanism for the synthesis of thiazolyl-pyrazoline Schiff base hybrids via ZnO nanoparticles as a catalyst was proposed as shown in Scheme 5.

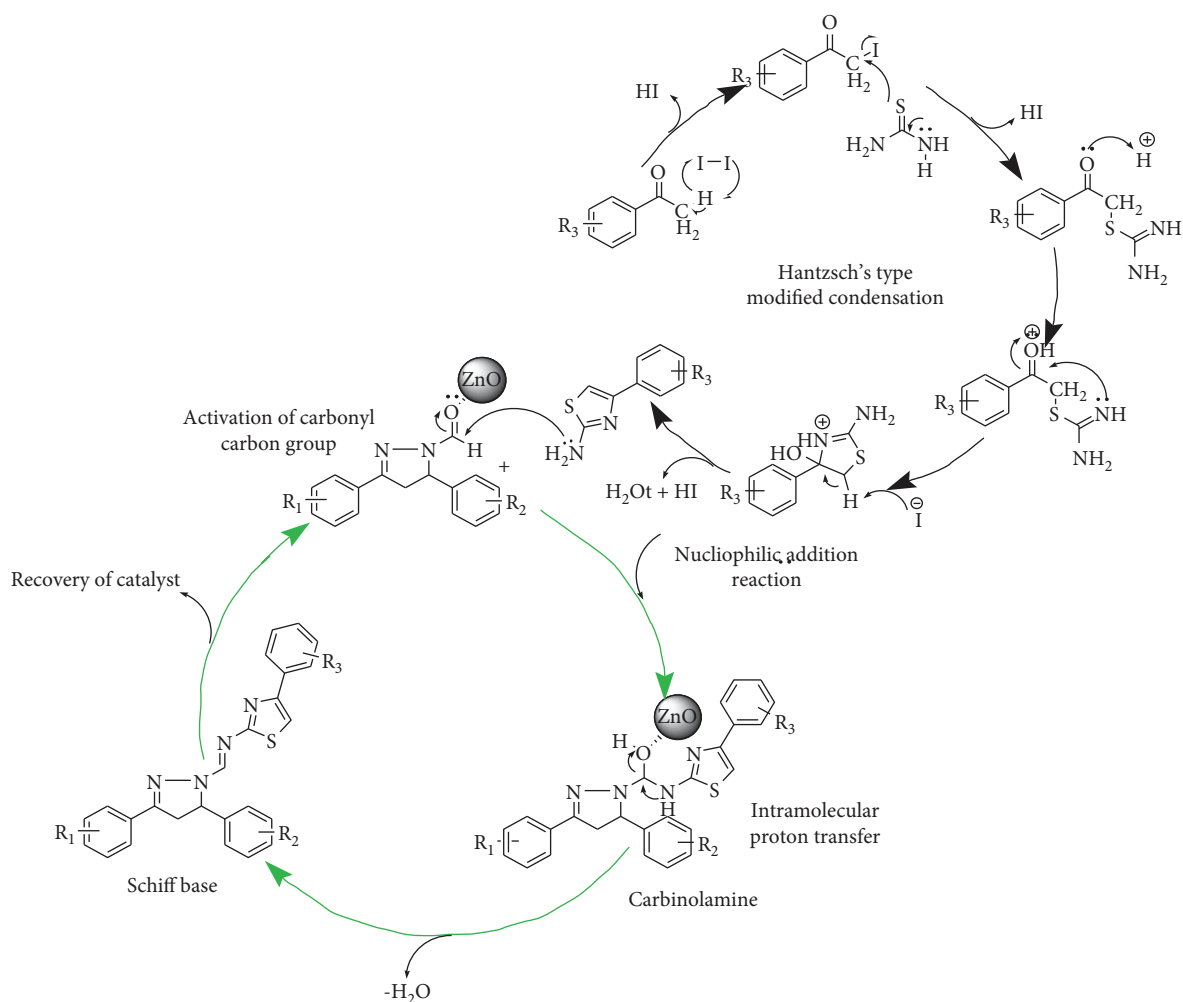
**3.3. In Vitro Antibacterial Activity.** The antibacterial activity of the synthesized thiazolyl-pyrazoline Schiff base hybrids (16–24) was evaluated by *in vitro* disk diffusion bioassay and measuring inhibition zone diameters (IZDs, expressed as mean  $\pm$  SD mm) at 500 and 250  $\mu$ g/mL against the following strains of bacteria: *Staphylococcus aureus* (ATCC 29213), *Streptococcus pyogenes* (ATCC 27853), *Escherichia coli* (ATCC 25922), and *Pseudomonas aeruginosa* (ATCC 27853) [39, 40]. Compounds 22 and 24 displayed potent inhibitory activity against *P. aeruginosa* ( $13.33 \pm 0.58$  mm and  $17.33 \pm 0.58$  mm, respectively) at 500  $\mu$ g/mL (Table 1) compared with amoxicillin ( $15.00 \pm 1.00$  mm). Compounds 19 and 24 displayed promising activity against *E. coli* ( $12.00 \pm 1.00$  mm and  $17.00 \pm 1.00$  mm, respectively) at 500  $\mu$ g/mL compared with amoxicillin ( $14.67 \pm 0.58$  mm). Compounds 18, 19, 21, and 24 displayed promising activity against *S. pyogenes* ( $19.33 \pm 0.58$  mm,  $19.33 \pm 0.58$  mm,  $18.67 \pm 2.52$  mm, and  $15.67 \pm 0.58$  mm, respectively) at 500  $\mu$ g/mL, whereas compounds 18 and 21 displayed promising activity against *S. aureus* ( $10.00 \pm 1.00$  mm and  $11.00 \pm 1.00$  mm, respectively) at 500  $\mu$ g/mL compared with amoxicillin ( $33.33 \pm 1.53$  mm and  $15.00 \pm 1.00$  mm, respectively). The rest of the compounds showed moderate to weak activity against the tested bacterial strains. Thus, these potent antibacterial compounds could be considered promising lead compounds to develop new antibacterial drugs (Figure 2, SI Appendix C Figure S6).

**3.3.1. Structure-Activity Relationships (SARs).** Structure-activity-based mechanism of antimicrobial action is critical for the design and improvement of novel antimicrobial and antioxidant agents. The results demonstrate that compound 17, with a *p*-NO<sub>2</sub> substituent on the aromatic ring of thiazole moiety, resulted in a decreasing pattern in antibacterial activity against all strains compared with compound 16, which has a hydrogen atom at *para* position of the aromatic ring of thiazole moiety. Compound 18, with a *p*-OH substituent on the aromatic ring of thiazole moiety, resulted in an increase in antibacterial activity towards *S. aureus* at 250  $\mu$ g/mL and *S. pyogenes* at 250 and 500  $\mu$ g/mL compared with compound 16. Compound 20, with a *p*-NO<sub>2</sub> substituent on the aromatic ring of thiazole moiety, resulted in an increase in antibacterial activity towards *S. aureus* at 500  $\mu$ g/mL and *S. pyogenes* at 250  $\mu$ g/mL compared with compound 19, which has hydrogen at the *para* position of the aromatic ring of thiazole moiety. Compound 21, with a *p*-OH substituent on the aromatic ring of thiazole moiety, resulted in an increase in antibacterial activity towards *S. aureus* and *S. pyogenes* at 500  $\mu$ g/mL compared with compound 19, which has hydrogen at the *para* position of the aromatic ring of thiazole moiety, whereas compound 23, with a *p*-NO<sub>2</sub> substituent on the aromatic ring of thiazole moiety, resulted in an increasing antibacterial activity trend towards *S. aureus* and *S. pyogenes* at 500  $\mu$ g/mL compared with compound 22. On the other hand, compound 21, with a *p*-OH substituent on the aromatic ring of thiazole moiety, resulted in an increase in antibacterial activity towards *S. pyogenes*, *E. coli*, and *P. aeruginosa* at 500  $\mu$ g/mL compared with compound 19, which has hydrogen at the *para* position of the aromatic ring of thiazole moiety. In addition, the presence of *p*-Br and *p*-OH group pyrazoline moiety bearing with substituted-phenyl rings might be the most relevant cause for enhancing the antibacterial activities. The results suggest that the antibacterial activity of the investigated compounds was influenced by the physicochemical properties of the type and position of substituent on the aromatic rings of thiazole and pyrazoline moieties.

### 3.4. Antioxidant Activities

**3.4.1. DPPH Free Radical Scavenging and Lipid Peroxidation Inhibition.** The antioxidant activity of compounds 16–24 was determined by the DPPH assay. From the results obtained (Table 2), only compound 21 displayed significant





SCHEME 5: A plausible mechanism for the synthesis of thiazolyl-pyrazoline Schiff base hybrids via ZnO nanoparticles as a catalyst.

antioxidant activity ( $IC_{50} = 4.63 \mu\text{g/mL}$ ) compared with the positive control, ascorbic acid ( $IC_{50} = 3.21 \mu\text{g/mL}$ ) (Figure 3). The rest of the compounds showed moderate to weak activity. Most of the synthesized compounds (except 17 and 22) showed greater than 80% of DPPH radical scavenging activity at a concentration of  $200 \mu\text{g/mL}$  (Figure 4). The presence of electron-donating hydroxyl functionality at an *ortho* position of thiazole phenyl groups could be the most possible reason, which might stabilize the radicals for their strong electron-donating nature [41]. Compounds 21 and 24 inhibited peroxide formation by  $80.01 \pm 0.07\%$  and  $79.44 \pm 0.05\%$ , respectively, demonstrating their potential in preventing lipid peroxide formation as presented (Table 2). Thus, the results showed that the studied thiazole-pyrazoline-based Schiff base hybrids remove the free radicals, especially the lipid peroxide radicals, by giving them their hydrogen atom and thus inhibiting the lipid peroxidation reaction.

**3.5. In Silico ADMET Prediction.** SwissADME is a Web-based tool that provides important information about drug-likeness and pharmacokinetic properties of bioactive

molecules [42, 43]. In this perspective, the theoretical agreement of synthesized compounds to Lipinski's rule of five and Veber's rule [30, 31, 44], as well as the pharmacokinetic and toxicity parameters, was estimated using ADMET descriptors by a SwissADME [31] and PreADMET [45] online servers. The percent absorption (%Abs) of the synthesized compounds was computed using the formula  $\% \text{Abs} = 109 - 0.345 \text{TPSA}$  [46]. The filter that combines Lipinski's "rule of five" refers physicochemical properties of a molecule to become a drug (i.e.,  $MW \leq 500$  Daltons,  $i\text{Log } P \leq 5$ , H-bond donors  $\leq 5$ , and H-bond acceptors  $\leq 10$ ) [44] and Veber's parameters ( $\text{TPSA} \leq 140 \text{ \AA}^2$  and rotatable bonds  $\leq 10$ ) [30]. ProTox-II Web server exploration was used to forecast the ligands' organ toxicity profiles and toxicological endpoints, as well as their  $LD_{50}$  [46, 47]. The results showed that all of the compounds obeyed Lipinski's rule of five (Table 3), with only minor deviations for 19–21 and 23, and thus, they have the potentials to be developed as orally bioavailable drugs. All synthesized compounds have a higher bioavailability score of 0.55 and were suitable for oral administration, indicating drug-like qualities [48]. Their HBD values are  $< 3$ , indicating that they are highly soluble in cellular membranes, with HBA values ranging from 5 to 8.

TABLE 1: Antibacterial activity of compounds 16–24 and amoxicillin against selected Gram-positive and Gram-negative strains.

Synthesized compounds	Concentration ( $\mu\text{g/mL}$ )	Mean inhibition zone diameter (IZD) in mm			
		Gram-positive bacteria		Gram-negative bacteria	
		<i>Staphylococcus aureus</i> (ATCC 29213)	<i>Streptococcus pyogenes</i> (ATCC 27853)	<i>Escherichia coli</i> (ATCC 25922)	<i>Pseudomonas aeruginosa</i> (ATCC 27853)
16	500	8.67 $\pm$ 0.58	9.00 $\pm$ 0.00	7.33 $\pm$ 0.58	8.67 $\pm$ 0.58
	250	8.33 $\pm$ 0.58	7.33 $\pm$ 0.58	6.67 $\pm$ 0.58	6.00 $\pm$ 0.00
17	500	8.33 $\pm$ 0.58	6.33 $\pm$ 0.58	6.00 $\pm$ 0.00	7.33 $\pm$ 1.15
	250	8.33 $\pm$ 0.58	6.00 $\pm$ 0.00	6.67 $\pm$ 0.58	8.00 $\pm$ 1.00
18	500	8.00 $\pm$ 1.00	19.33 $\pm$ 0.58	6.67 $\pm$ 0.58	7.33 $\pm$ 0.58
	250	10.00 $\pm$ 1.00	18.33 $\pm$ 0.58	6.00 $\pm$ 0.00	6.67 $\pm$ 0.58
19	500	7.33 $\pm$ 0.58	19.33 $\pm$ 0.58	12.00 $\pm$ 1.00	9.67 $\pm$ 0.58
	250	6.33 $\pm$ 0.58	17.00 $\pm$ 1.00	9.33 $\pm$ 0.58	8.00 $\pm$ 1.00
20	500	9.00 $\pm$ 0.00	8.00 $\pm$ 1.00	7.67 $\pm$ 0.58	7.33 $\pm$ 0.58
	250	8.33 $\pm$ 0.58	14.00 $\pm$ 2.00	7.00 $\pm$ 0.00	7.33 $\pm$ 0.58
21	500	11.00 $\pm$ 1.00	18.67 $\pm$ 2.52	8.00 $\pm$ 0.00	7.33 $\pm$ 0.58
	250	11.67 $\pm$ 0.58	22.33 $\pm$ 1.53	6.33 $\pm$ 0.58	7.00 $\pm$ 0.00
22	500	6.67 $\pm$ 0.58	6.00 $\pm$ 0.00	13.33 $\pm$ 0.58	13.33 $\pm$ 0.58
	250	7.00 $\pm$ 0.00	6.00 $\pm$ 0.00	11.33 $\pm$ 0.58	7.00 $\pm$ 1.00
23	500	9.67 $\pm$ 0.58	9.67 $\pm$ 0.58	6.00 $\pm$ 0.00	8.00 $\pm$ 2.00
	250	8.67 $\pm$ 0.58	7.00 $\pm$ 0.00	8.00 $\pm$ 0.00	8.00 $\pm$ 1.00
24	500	8.33 $\pm$ 0.58	15.67 $\pm$ 0.58	17.00 $\pm$ 1.00	17.33 $\pm$ 0.58
	250	7.67 $\pm$ 0.58	10.67 $\pm$ 0.58	8.00 $\pm$ 0.00	18.67 $\pm$ 0.58
Amoxicillin	500	15.00 $\pm$ 1.00	33.33 $\pm$ 1.53	14.67 $\pm$ 0.58	15.00 $\pm$ 1.00
	250	14.00 $\pm$ 1.00	29.67 $\pm$ 2.52	10.33 $\pm$ 0.58	14.33 $\pm$ 2.52
DMSO		6 $\pm$ 0.00	6 $\pm$ 0.00	6 $\pm$ 0.00	6 $\pm$ 0.00

<sup>a</sup>The experiment was carried out in triplicate and the average zone of inhibition was calculated. <sup>b</sup>ATCC: American Tissue Culture Collection. <sup>c</sup>IZD, inhibition zone diameter.

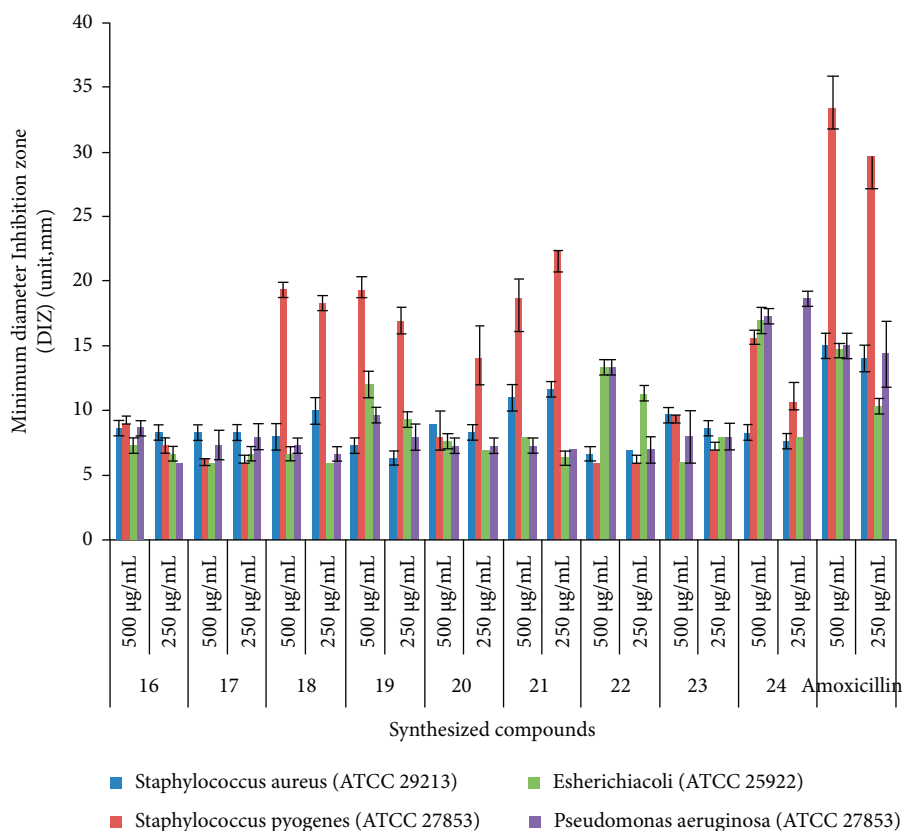


FIGURE 2: Minimum diameter inhibition zone of the synthetic compounds (16-24) in mm (mean  $\pm$  SD) at 250 and 500  $\mu\text{g/mL}$  concentrations.

TABLE 2: *In vitro* antioxidant and anti-lipid peroxidation inhibition test with various concentrations of 16–24.

Conc. ( $\mu\text{g/mL}$ )	% of inhibition of the synthesized compounds*														Ascorbic acid <sup>a</sup>
	16	17	18	19	20	21	22	23	24	25	26	27	28	29	
12.5	32.32 $\pm$ 0.50	22.75 $\pm$ 0.31	29.67 $\pm$ 0.24	22.69 $\pm$ 0.54	19.00 $\pm$ 0.01	35.32 $\pm$ 0.03	18.13 $\pm$ 0.55	25.96 $\pm$ 0.08	34.02 $\pm$ 0.02	38.94 $\pm$ 0.04					
25.0	47.25 $\pm$ 0.36	33.59 $\pm$ 0.41	40.95 $\pm$ 0.12	44.90 $\pm$ 0.02	32.73 $\pm$ 0.11	55.73 $\pm$ 0.04	33.82 $\pm$ 0.36	38.99 $\pm$ 0.07	49.63 $\pm$ 0.25	57.16 $\pm$ 0.13					
50.0	63.9 $\pm$ 0.30	56.0 $\pm$ 0.36	67.9 $\pm$ 0.16	60.2 $\pm$ 0.20	55.4 $\pm$ 0.39	76.3 $\pm$ 0.11	56.9 $\pm$ 0.41	58.1 $\pm$ 0.28	62.9 $\pm$ 0.16	77.6 $\pm$ 0.18					
100.0	74.33 $\pm$ 0.29	68.21 $\pm$ 0.74	76.92 $\pm$ 0.03	77.61 $\pm$ 0.06	78.92 $\pm$ 0.04	80.44 $\pm$ 0.11	67.83 $\pm$ 0.11	73.19 $\pm$ 0.21	77.53 $\pm$ 0.34	83.73 $\pm$ 0.06					
200.0	80.25 $\pm$ 0.35	78.44 $\pm$ 0.38	83.74 $\pm$ 0.17	81.22 $\pm$ 0.14	85.74 $\pm$ 0.23	91.49 $\pm$ 0.05	78.45 $\pm$ 0.30	80.53 $\pm$ 0.13	87.41 $\pm$ 0.02	95.71 $\pm$ 0.13					
IC <sub>50</sub> ( $\mu\text{g/mL}$ )*	34.25	70.93	39.79	27.34	64.62	4.63	27.32	57.35	29.08	3.21					
% Anti-lipid peroxidation inhibition	55.74 $\pm$ 0.09	68.05 $\pm$ 0.54	65.00 $\pm$ 0.14	70.66 $\pm$ 0.52	69.07 $\pm$ 0.52	80.01 $\pm$ 0.07	58.88 $\pm$ 0.25	69.66 $\pm$ 0.11	79.44 $\pm$ 0.05						

\*IC<sub>50</sub> is the 50% inhibitory concentration of the samples, and the results were represented as mean  $\pm$  SD. <sup>a</sup> Ascorbic acid was used as a positive control.

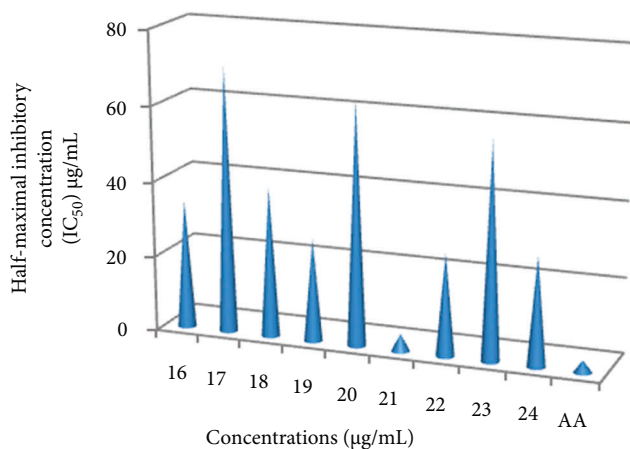


FIGURE 3: Half-maximal inhibitory concentration ( $IC_{50}$ ) of synthesized compounds (16–24) as compared to that of ascorbic acid.

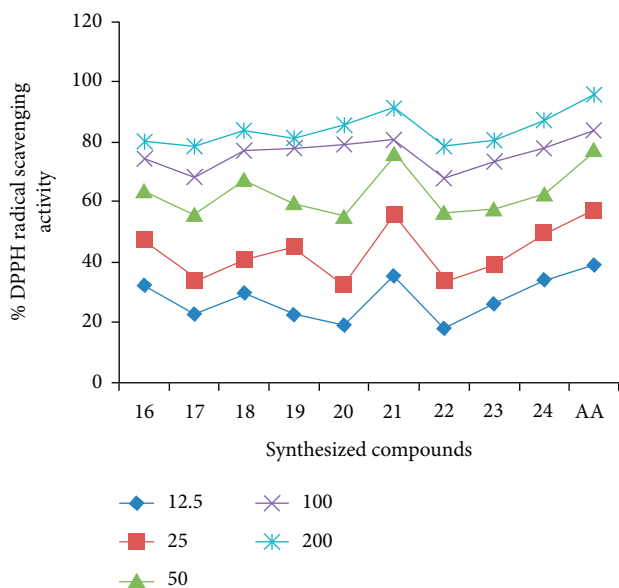


FIGURE 4: % inhibition of the synthesized compounds (16–24) and the standard drug at different concentration ranges.

The  $i\text{LogP}$  values for all compounds are  $<5$ , notably for 20 and 22–24 indicating the compounds have good lipophilicity characteristics, which may protect them against ROS degradation.  $\text{TPSA}$  ranged from 86.68 to 152.73  $\text{\AA}^2$ , while the consensus  $\log P_{\text{O/W}}$  (indicator of lipophilicity) was observed in an optimal range from 2.06 to 3.64. Compounds that satisfy the parameters of  $\text{TPSA} \leq 140 \text{\AA}^2$  are expected to have adequate solubility, oral bioavailability, and cell permeability [49]. All compounds (16–24) exhibited better percent absorption (% Abs) than amoxicillin suggesting good oral bioavailability.

*In silico* pharmacokinetic characteristic results (Table 4) revealed that compounds 16–24 had superior intestinal absorption to amoxicillin, ranging from 90.80 to 99.82% absorption with HIA values near 100%. *In vitro*, Caco2 and MDCK cells have moderate to high permeability, notably 18, 22, and 24, and especially 19 and 24, which are better than

amoxicillin (0.39), respectively. Skin permeability (SP,  $\text{Log}_{\text{Kp}}$ ) was found to be somewhat below the permitted range of  $-5.42$  to  $-6.59$  cm/sec, and a substance with a low negative  $\text{Log}_{\text{Kp}}$  value has higher absorption into human skin. The results indicate that the synthesized compounds are showing good absorption properties to cross the gut wall by passive diffusion mechanism to reach the target. All of the compounds were poorly absorbed into the CNS *in vivo*, showing that they have a decreased ability to cross the CNS, with a total clearance value of 24 (0.07), which is comparable to amoxicillin (0.06). All of the substances have a high PPB%, with values of more than 90%, suggesting that they are strongly bound. The results revealed that compounds 18 (99.75) and 24 (97.31) had high PPB values, indicating longer half-lives than amoxicillin (23.35) [50]. Furthermore, glycoprotein (P-gp) inhibition measurements are utilized to forecast the target drugs' excretion properties. P-gp and cytochrome P450 (CYP) are known to aid in the protective efflux (biotransformation) of biological membranes (GI tract or brain) from xenobiotics to protect tissues [51]. The compounds' metabolic properties were predicted by the behavior of cytochrome P450 and their isoform enzymes. In this investigation, compounds 16–24 showed no inhibitory activity against CYP2C19, CYP2C9, CYP2C6, or CYP3A4, except 3b and 3c, which showed inhibitory activity against CYP2D9. In our study, none of the synthesized compounds inhibited P-gp substrates, except 16 and 19.

Toxicity data must be connected with *in vitro* safety investigations before being examined in relevant laboratory animal models [52]. In addition, all compounds were predicted for their computational toxicity risks, such as the AMES test (for mutagenicity prediction), tumorigenicity carcino-mouse/rat (for carcinogenicity prediction), and skin irritancy hERG inhibition (for checking cardiac toxicity), and cytotoxicity effect (Table 5). Based on toxicity profiles, all compounds (16–24) and amoxicillin showed mutagenic behavior in the AMES test. All compounds, except for 17, 20, 23, 24, and amoxicillin, exhibited no possible carcinogenic effect in mice and no potential carcinogenic effect in rats. All of the compounds exhibited a low risk of being cardiotoxic or cytotoxic, as well as being safer than standard drugs. All of the synthesized compounds tested had predicted  $\text{LD}_{50}$  (mg/kg) values ranging from 800 to 1,000 putting them in ProTox-II class 4, indicating that they could be harmful if swallowed ( $300\text{LD}_{50} \leq 2000$ ) [53]. The bioavailability radar plots of the tested compounds (16–24) indicated that all of the compounds were completely within the pink area, indicating that they have drug-like qualities with an improved bioavailability profile (SI Appendix C Figure S7) [54]. Even though the chemical violates type Fsp3<sup>0.25</sup>, unsaturation score (INSATU), it is verifiable that it does not violate any of Lipinski and Veber's standards, satisfying the qualifications within the ideal spectrum that combines drug-likeness criteria. Using  $w\text{LogP}$  and  $\text{TPSA}$ , the BOILED-Egg server predicts this pharmacokinetics [55]. As a result, pharmacokinetics were evaluated using the BOILED-Egg model, which appeared in the white ellipse (HIA) justifying their high probability of being passively absorbed by the gastrointestinal tract, with red points for 18, 21, and 24 (non-

TABLE 3: Parameters of in silico bioavailability prediction and physicochemical properties of compounds (16–24) and amoxicillin.

Compound	MW	iLogP	HBD (n <sub>OHNH</sub> )	HBA (n <sub>ON</sub> )	n rotb	MR	TPSA	% ABS	Lipinski #violations	Bioavailability score
Lipinski*	≤500	≤5	≤5	≤10	≤10	—	—	100%		
Veber**	—	—	—	—	—	—	≤140			
16	453.52	3.64	0	5	6	140.68	86.68	79.09	0	0.55
17	498.51	3.31	0	7	7	149.51	132.51	63.28	0	0.55
18	469.52	3.09	1	6	6	142.71	106.91	72.11	0	0.55
19	532.41	3.23	0	5	6	148.38	86.68	79.09	1	0.55
20	577.41	2.81	0	7	7	157.21	132.51	63.28	1	0.55
21	548.41	3.54	1	6	6	150.41	106.91	72.11	1	0.55
22	469.52	2.66	1	6	6	142.71	106.91	72.11	0	0.55
23	514.51	2.06	1	8	7	151.53	152.73	56.30	1	0.17
24	485.51	2.57	2	7	6	144.73	127.14	65.13	0	0.55
Amoxicillin	365.4	1.46	4	6	6	94.59	132.96	63.12	0	0.55

\*Reference values of Lipinski; \*\*reference values of Veber; (–): not tested. MW, molecular weight; iLogP, lipophilicity (O/W, octanol-water partitioning coefficient); HBD, number of hydrogen bond donors (OH and NH groups); HBA, number of hydrogen bond acceptors (O and N atoms); nVs, number of Lipinski rule violations; n rotb, number of rotatable bonds; MR, molar refractivity; TPSA, topological polar surface area; (Å<sup>2</sup>); %ABS, percentage of absorption (%Abs = 109 – (0.345 × TPSA)).

TABLE 4: Pharmacokinetic (ADME) property prediction of compounds (16–24) and amoxicillin using PreADMET online server.

Compound	Absorption				Distribution		Metabolism and excretion				
	HIA (%) <sup>a</sup>	Caco2 (nm/sec) <sup>b</sup>	SP, Log <sub>K<sub>p</sub></sub> (cm/hour) <sup>c</sup>	MDCK (nm/sec) <sup>d</sup>	PPB % <sup>e</sup>	BBB (c.brain/c.blood) <sup>f</sup>	CYP2C19 <sup>g</sup>	CYP2C9 <sup>h</sup>	CYP2D6 <sup>i</sup>	CYP3A4 <sup>j</sup>	P-gp_inhibition <sup>k</sup>
16	99.82	15.60	–5.80	0.047	96.53	0.80	Non	Non	Non	Non	Inhibitor
17	96.14	9.39	–5.81	0.047	95.90	0.21	Non	Non	Non	Non	Non
18	98.56	4.35	–5.61	0.044	99.75	0.34	Non	Non	Non	Non	Non
19	98.43	27.34	–6.59	0.021*	93.54	1.59	Non	Non	Non	Non	Inhibitor
20	99.40	17.52	–6.60	0.018*	93.82	0.41	Non	Non	Non	Non	Non
21	98.02	18.88	–6.40	0.030*	93.30	0.63	Non	Non	Non	Non	Non
22	98.56	7.78	–5.61	0.044	94.41	0.24	Non	Non	Non	Non	Non
23	90.80	11.84	–5.62	0.044	94.60	0.12	Non	Inhibitor	Non	Non	Non
24	95.95	5.52	–5.42	0.044	97.31	0.07	Non	Inhibitor	Non	Non	Non
Amoxicillin	62.93	0.34	–0.21	0.398	23.35	0.06	Non	Non	Inhibitor	Non	Non

<sup>a</sup> HIA : human intestinal absorption; <sup>b</sup> Caco2: Caco2 cell permeability; <sup>c</sup> SP, Log<sub>K<sub>p</sub></sub>: skin permeability; <sup>d</sup> MDCK : Madin–Darby canine kidney; <sup>e</sup> PPB : plasma protein binding; <sup>f</sup> BBB level: blood-brain barrier level; <sup>g-h</sup> CYP2D6 : cytochrome P; <sup>k</sup> P-gp: glycoprotein inhibition.

TABLE 5: *In silico* toxicity prediction of compounds (16–24) and amoxicillin using PreADMET and ProTox-II protocols.

Compound	Toxicity						Class
	AMES (mutagenicity prediction)	Carcino_mouse (for carcinogenicity prediction of the tested compounds)	Carcino_rat (for carcinogenicity prediction of the tested compounds)	hERG_inhibition (for checking the cardiac toxicity)	Cytotoxicity	<sup>a</sup> LD <sub>50</sub> (mg/kg)	
16	Mutagen	Negative	Positive	low_risk	Negative	1000	4
17	Mutagen	Positive	Positive	low_risk	Negative	1000	4
18	Mutagen	Negative	Positive	low_risk	Negative	800	4
19	Mutagen	Negative	Positive	low_risk	Negative	800	4
20	Mutagen	Positive	Positive	low_risk	Negative	1000	4
21	Mutagen	Negative	Positive	low_risk	Negative	800	4
22	Mutagen	Negative	Positive	low_risk	Negative	800	4
23	Mutagen	Positive	Negative	low_risk	Negative	800	4
24	Mutagen	Negative	Negative	low_risk	Negative	1000	4
Amoxicillin	Mutagen	Positive	Negative	low_risk	Negative	15000	4

<sup>a</sup>LD<sub>50</sub>: lethal dose parameter.

substrate of P-gp) and blue points for 16 and 19 (substrate of P-gp), respectively (SI Appendix C Figure S8). They were predicted to be no P-gp substrate, despite their promising intestinal absorption and bioavailability, and they cannot pass through the blood-brain barrier (BBB), demonstrating they are not able to cross the blood-brain barrier to the brain when it attaches to certain receptors.

**3.6. In Silico Molecular Docking Simulation.** Studies of docking simulations were carried out to identify the binding pattern of the synthesized compounds (16–24) to selected protein target active sites (i.e., DNA gyrase B, PqsA, pyruvate kinase, LuxS, and human peroxiredoxin 5) [56]. The binding affinity, hydrogen bond, and amino acid residual interactions (hydrophobic/ $\pi$ -cation/ $\pi$ -anion/ $\pi$ -alkyl and van der Waals interactions) of ligands (16–24) and standards are presented (SI Tables 7–11). The majority of the hybrids investigated had the best docking scores and good interactions (2D and 3D) with different amino acid residues (SI Appendix D Figure S5(a)–S5(e), 1–10).

**3.6.1. Molecular Docking Studies of Synthesized Compounds (16–24) against *E. coli* DNA Gyrase B (PDB ID: 6f86).** The synthesized compounds (16–24) were docked towards the bacterial DNA gyrase B receptor to determine their binding affinity, and the results were compared to amoxicillin (SI Appendix D Figure S5(a), 1–10, and Table S7) [57]. The minimum binding energies of the synthesized compounds (16–24) ranged from  $-7.4$  to  $-8.5$  kcal/mol, showing that thiazolyl-pyrazoline Schiff base hybrids have a thermodynamically favorable inhibitory action on *E. coli* DNA gyrase B. Compounds 19 ( $-8.0$  Kcal/mol), 20 ( $-7.8$  Kcal/mol), 21 ( $-7.9$  Kcal/mol), 22 ( $-8.5$  Kcal/mol), and 24 ( $-7.9$  Kcal/mol) have high binding interactions with DNA gyrase B, respectively (SI Figure 5 and SI Appendix D Figure 5(a), 10) compared with amoxicillin ( $-7.1$  Kcal/mol). The synthesized compounds displayed similar residual interactions with amino acid residues of Ile-78 and Ile-94, as well as hydrogen bonding interaction patterns with Val-120, Asn-46, and Ser-121 when compared to standard amoxicillin. The docking results (high negative binding affinity) are in good agreement with the *in vitro* antibacterial results of compounds 19, 22, and 24 against Gram-negative *E. coli* bacteria.

**3.6.2. Molecular Docking Studies of Synthesized Compounds (16–24) against the N-Terminal Domain of PqsA in a Complex with 6-Fluoroanthraniloyl-AMP (PDB ID:5oe3).** The binding affinity of synthesized compounds (16–24) was evaluated towards the N-terminal domain of PqsA in the 6-fluoroanthranilamidoyl-AMP complex [58] and compared with amoxicillin (SI Appendix D Figure S5(b), 1–10, and Table S8). The synthesized compounds (16–24) have minimum binding energy in the binding pocket of the N-terminal domain of PqsA ranging from  $-7.8$  to  $-10.7$  kcal/mol.

Compounds 17 ( $-9.5$  Kcal/mol), 19 ( $-9.6$  Kcal/mol), 20 ( $-9.5$  Kcal/mol), 22 ( $-10.7$  Kcal/mol), 23 ( $-9.6$  Kcal/mol), and 24 ( $-9.9$  Kcal/mol) have large binding interactions. Higher binding affinity was observed for compounds 22 and 24, with the binding affinity of  $-10.7$  and  $-9.9$  Kcal/mol, respectively, against PqsA compared with amoxicillin ( $-7.3$  Kcal/mol), suggesting that the compounds are promising antibacterial agents against *P. aeruginosa* (Figure 6 and SI Appendix D Figure 5(b), 10), in good agreement with the *in vitro* antibacterial activity against Gram-negative *P. aeruginosa* observed. The synthesized compounds revealed similar amino acid residue interactions with Thr-232, Arg-128, Asp-231, Asp-132, Ala-124, Ala-126, Phe-209, Gly-302, and H-bonding interaction profiles with Asn-61, Ser-65, and Pro-129 as compared to the amoxicillin drug.

**3.6.3. Molecular Docking Studies of Synthesized Compounds (16–24) against *S. aureus* Pyruvate Kinase (PDB ID:3t07).** The synthesized compounds (16–24) were subjected to a molecular docking analysis to determine their binding affinity towards pyruvate kinase in a complex containing the natural bisindole alkaloid, and the results were compared to amoxicillin (SI Appendix D Figure S5(c), 1–10, and Table S9) [59,60]. It was found that the synthesized compounds have minimum binding energy in the range of  $-4.8$  to  $-6.4$  kcal/mol. Compounds 18 ( $-5.5$  Kcal/mol), 19 ( $-5.0$  Kcal/mol), 20 ( $-5.5$  Kcal/mol), 21 ( $-5.2$  Kcal/mol), 22 ( $-5.9$  Kcal/mol), 23 ( $-6.4$  Kcal/mol), and 24 ( $-5.0$  Kcal/mol) have better binding interactions, with the best docking score obtained for compounds 21, 22, and 23 with binding affinity of  $-5.2$ ,  $-5.9$ , and  $-6.4$  Kcal/mol, respectively, against pyruvate kinase compared with amoxicillin ( $-4.7$  Kcal/mol) (Figure 7 and SI Appendix D Figure 5(c), 10). This suggests that these compounds are effective antibacterial agents against *S. aureus*. Amino acid residue interactions with Pro-402, Lys-425, Leu-355, Ile359, and H-bonding interaction patterns with Ala-358, Thr-464, Gly-462, and Ser-383 were similar in the synthesized compounds. The *in vitro* biological results of 21 against Gram-positive bacteria of *S. aureus* are in good agreement with molecular docking results to some extent.

**3.6.4. Molecular Docking Studies of Synthesized Compounds (16–24) against LuxS of *S. pyogenes* (UniProt Id: P0C0C7).** The binding affinity of synthesized compounds (16–24) was examined against LuxS and compared with amoxicillin (SI Appendix D Figure S5d, 1–10, and Table S10) [61]. The synthesized compounds (16–24) had minimal binding energies ranging from  $-3.7$  to  $-5.1$  kcal/mol (SI Table S10). The binding affinity of 21 against LuxS was nearly identical ( $-5.1$  Kcal/mol) to that of amoxicillin ( $-5.5$  Kcal/mol), indicating that these compound is promising antibacterial agents against *S. pyogenes* (Figure 8 and SI Appendix D Figure 5d, 10), in good agreement with the *in vitro* biological results of observed by 21 against Gram-positive bacteria of *S. pyogenes*. The synthesized compounds have similar amino



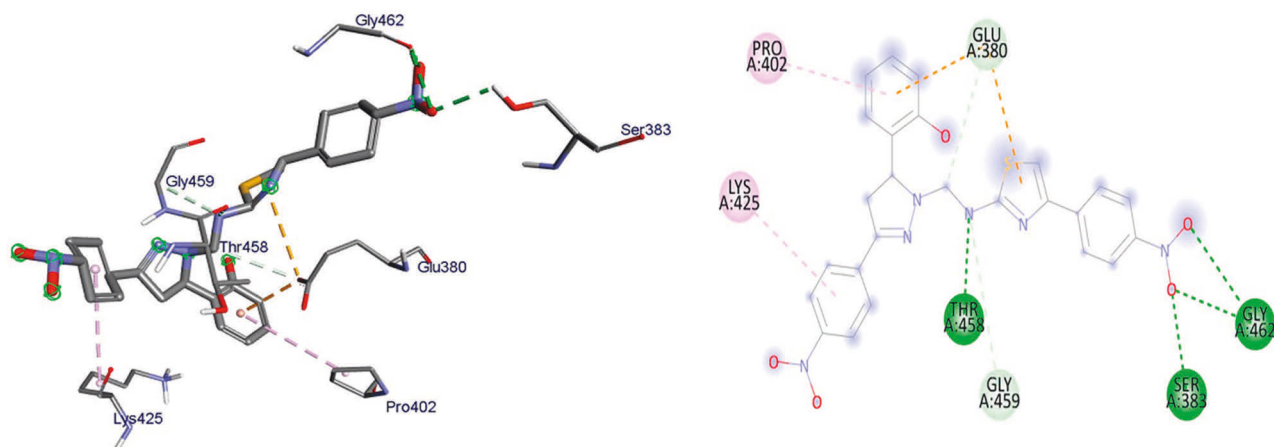


FIGURE 7: 3D (a) and 2D (b) representations of the binding interactions of 23 against *S. aureus* pyruvate kinase.

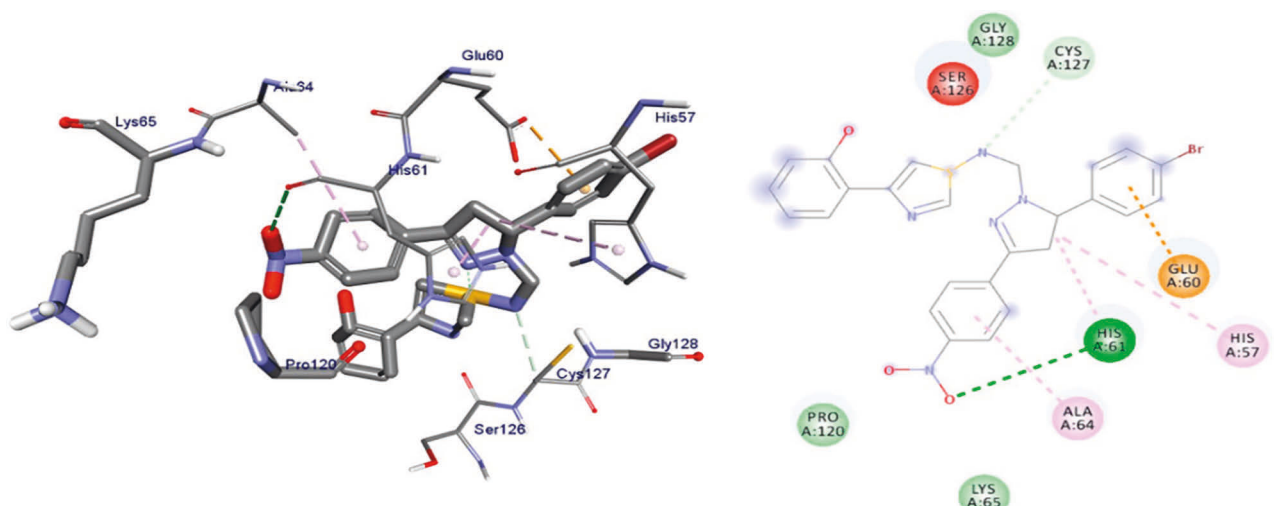


FIGURE 8: 3D (a) and 2D (b) representations of the binding interactions of 21 against LuxS of *S. pyogenes*.

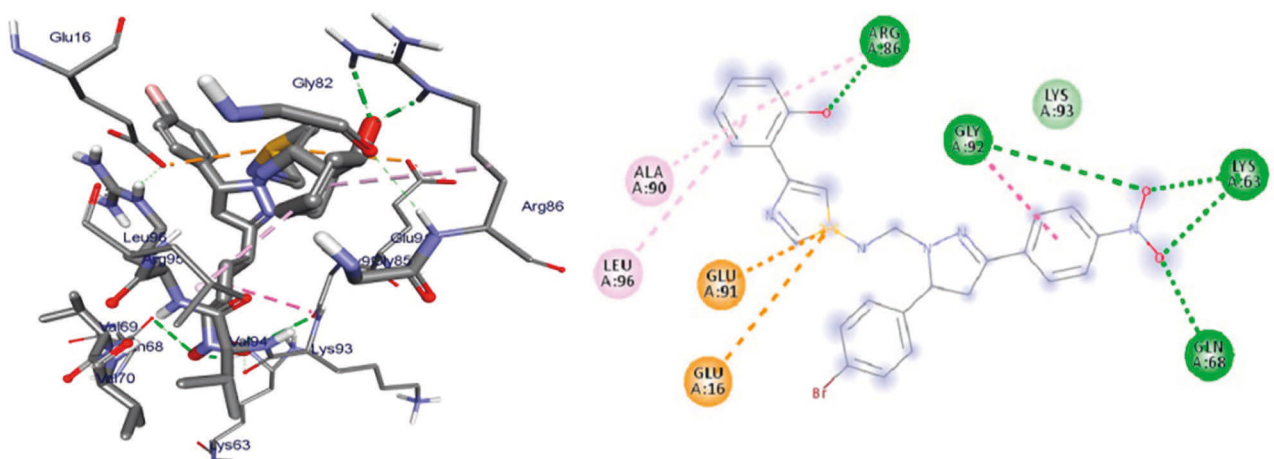


FIGURE 9: 3D (a) and 2D (b) representations of the binding interactions of 21 against human peroxiredoxin 5.



#### 4. Conclusion and Future Outlooks

In this study, we reported the conventional and green synthesis of nine thiazolyl-pyrazoline Schiff base hybrids together with their ADMET profile predictions and molecular docking study as antibacterial and antioxidant agents. The structures of the synthesized compounds were determined using combined spectroscopic techniques (UV-Vis,  $^1\text{H-NMR}$ , and  $^{13}\text{C-NMR}$ ). The results of antibacterial screening indicate that compound 24 (IZD =  $18.67 \pm 0.58$  mm) was more potent than amoxicillin (IZD =  $14.33 \pm 2.52$  mm) against *P. aeruginosa* at 250  $\mu\text{g/mL}$ , whereas compounds 22 and 24 (IZD =  $13.33 \pm 0.58$  mm and  $17.00 \pm 1.00$  mm, respectively) showed better activity compared with amoxicillin (IZD =  $14.67 \pm 0.58$  mm) at 500  $\mu\text{g/mL}$  against *E. coli*. The remaining compounds showed moderate to weak activity against the tested bacterial strains. Compound 21 displayed significant inhibition of DPPH ( $\text{IC}_{50} = 4.63$   $\mu\text{g/mL}$ ) compared with ascorbic acid ( $\text{IC}_{50} = 3.21$   $\mu\text{g/mL}$ ). Compound 21 displayed  $80.01 \pm 0.07\%$  inhibition of peroxide formation, suggesting its potential in preventing the formation of lipid peroxides. The results of the ADMET study showed that all synthesized compounds obeyed Lipinski's rule of five. *In silico* pharmacokinetic study demonstrated that compound 24 had superior intestinal absorption compared with amoxicillin.

Compounds 22 and 24 displayed binding affinities of -10.7 and -9.9 Kcal/mol, respectively, against PqsA compared with amoxicillin (-7.3 Kcal/mol) in agreement with the observed *in vitro* antibacterial activity against *P. aeruginosa*. Compound 21 displayed a binding affinity of -5.1 Kcal/mol and -7.8 Kcal/mol with LuxS and human peroxiredoxin 5, respectively, compared with amoxicillin and ascorbic acid (-5.5 and -5.2 Kcal/mol, respectively). Compounds 22 and 24 displayed higher binding affinity (-8.5 and -7.9 Kcal/mol, respectively) with DNA gyrase B compared with amoxicillin (-7.1 Kcal/mol). *In silico* toxicity study showed that all synthesized compounds had  $\text{LD}_{50}$  (mg/kg) values ranging from 800 to 1,000 putting them in ProTox-II class 4. The *in vitro* antibacterial activity and molecular docking analysis showed that compound 24 is a promising antibacterial therapeutic agent against *P. aeruginosa* and *E. coli*, whereas compound 22 is a promising antibacterial agent against *E. coli*. Compound 21 is found to be a promising antioxidant agent. Moreover, the green synthesis approach using ZnO nanoparticles as catalysts was found to be a very efficient method to synthesize biologically active thiazole-pyrazoline Schiff base hybrids compared with the conventional method. Future attempts should be carried out to synthesize a series of related thiazole-based Schiff base hybrids for comprehensive structure-activity relationship and *in vivo* studies to develop lead antioxidant and antibacterial drugs.

#### Data Availability

The data used to support the findings of this study are included within the manuscript and supplementary information.

#### Conflicts of Interest

The authors declare that they have no conflicts of interest regarding the publication of this study.

#### Acknowledgments

Demis Zelelew acknowledges the Department of Applied Chemistry, School of Applied Natural Science, Adama Science and Technology University, and Wachemo University for PhD opportunity study and leave of absence, respectively. The support rendered by Adama Public Health Research and Referral Laboratory Center, Adama, Ethiopia, during the antibacterial study is gratefully acknowledged.

#### Supplementary Materials

The UV-visible,  $^1\text{H}$ , and  $^{13}\text{C-NMR}$  spectra of all synthesized compounds, molecular docking scores, and 3D and 2D representations of the binding interactions of synthesized compounds (16–24) and amoxicillin/ascorbic acid against target proteins (i.e., DNA gyrase B, PqsA, pyruvate kinase, LuxS, and human peroxiredoxin 5), bioavailability radar, and BOILED-Egg model of the compounds (16–24) are all presented in the supplementary information. (*Supplementary Materials*)

#### References

- [1] R. J. Fair and Y. Tor, "Antibiotics and bacterial resistance in the 21st century," *Perspectives in Medicinal Chemistry*, vol. 6, 2014.
- [2] Á. Mourenza, J. A. Gil, L. M. Mateos, and M. Letek, "Oxidative stress-generating antimicrobials, a novel strategy to overcome antibacterial resistance," *Antioxidants*, vol. 9, no. 5, p. 361, 2020.
- [3] S. Mishra, S. Mishra, and P. Singh, "Hybrid molecules: the privileged scaffolds for various pharmaceuticals," *European Journal of Medicinal Chemistry*, vol. 124, pp. 500–536, 2016.
- [4] S. K. Konidala, V. Kotra, R. C. S. R. Danduga, P. K. Kola, R. B. Bhandare, and A. B. Shaik, "Design, multistep synthesis and *in vitro* antimicrobial and antioxidant screening of coumarin clubbed chalcone hybrids through molecular hybridization approach," *Arabian Journal of Chemistry*, vol. 14, no. 6, Article ID 103154, 2021.
- [5] A. Petrou, M. Fesatidou, and A. Geronikaki, "Thiazole ring—a biologically active scaffold," *Molecules*, vol. 26, no. 11, Article ID 3166, 2021.
- [6] B. Nehra, S. Rulhania, S. Jaswal, B. Kumar, G. Singh, and V. Monga, "Recent advancements in the development of bioactive pyrazoline derivatives," *European Journal of Medicinal Chemistry*, vol. 205, Article ID 112666, 2020.
- [7] A. Ayati, S. Emami, A. Asadipour, A. Shafee, and A. Foroumadi, "Recent applications of 1, 3-thiazole core structure in the identification of new lead compounds and drug discovery," *European Journal of Medicinal Chemistry*, vol. 97, pp. 699–718, 2015.
- [8] R. E. Khidre and I. A. M. Radini, "Design, synthesis and docking studies of novel thiazole derivatives incorporating pyridine moiety and assessment as antimicrobial agents," *Scientific Reports*, vol. 11, no. 1, 2021.

- [9] K. M. Dawood, T. M. Eldebss, H. S. El-Zahabi, and M. H. Yousef, "Synthesis and antiviral activity of some new bis-1, 3-thiazole derivatives," *European Journal of Medicinal Chemistry*, vol. 102, pp. 266–276, 2015.
- [10] M. Gollapalli, M. Taha, M. T. Javid et al., "Synthesis of benzothiazole derivatives as a potent  $\alpha$ -glucosidase inhibitor," *Bioorganic Chemistry*, vol. 85, pp. 33–48, 2019.
- [11] A. A. Siddiqui, S. Partap, S. Khisal, M. S. Yar, and R. Mishra, "Synthesis, anti-convulsant activity and molecular docking study of novel thiazole pyridazinone hybrid analogues," *Bioorganic Chemistry*, vol. 99, Article ID 103584, 2020.
- [12] V. Jaishree, N. Ramdas, J. Sachin, and B. Ramesh, "In vitro antioxidant properties of new thiazole derivatives," *Journal of Saudi Chemical Society*, vol. 16, no. 4, pp. 371–376, 2012.
- [13] H. Kasralikar, S. Jadhavar, S. Goswami, N. Kaminwar, and S. Bhusare, "Design, synthesis and molecular docking of pyrazolo [3, 4d] thiazole hybrids as potential anti-HIV-1 NNRT inhibitors," *Bioorganic Chemistry*, vol. 86, pp. 437–444, 2019.
- [14] M. Modrić, M. Bozicevic, I. Faraho, M. Bosnar, and I. Skoric, "Design, synthesis and biological evaluation of new 1, 3-thiazole derivatives as potential anti-inflammatory agents," *Journal of Molecular Structure*, vol. 1239, Article ID 130526, 2021.
- [15] G. Ghotbi, M. Mahdavi, Z. Najafi et al., "Design, synthesis, biological evaluation, and docking study of novel dual-acting thiazole-pyridiniums inhibiting acetylcholinesterase and  $\beta$ -amyloid aggregation for Alzheimer's disease," *Bioorganic Chemistry*, vol. 103, Article ID 104186, 2020.
- [16] C. Kesari, K. R. Rama, K. Sedighi et al., "Synthesis of thiazole linked chalcones and their pyrimidine analogues as anticancer agents," *Synthetic Communications*, vol. 51, no. 9, 2021.
- [17] M. Rana, R. Arif, F. I. Khan et al., "Pyrazoline analogs as potential anticancer agents and their apoptosis, molecular docking, MD simulation, DNA binding and antioxidant studies," *Bioorganic Chemistry*, vol. 108, Article ID 104665, 2021.
- [18] F. Tok, B. Irem Abas, O. Cevik, and B. Kocyigit-Kaymakcioglu, "Design, synthesis and biological evaluation of some new 2-Pyrazoline derivatives as potential anticancer agents," *Bioorganic Chemistry*, vol. 102, Article ID 104063, 2020.
- [19] B. Banerjee, "Recent developments on nano-ZnO catalyzed synthesis of bioactive heterocycles," *Journal of Nanostructure in Chemistry*, vol. 7, no. 4, pp. 389–413, 2017.
- [20] M. G. Demissie, F. K. Sabir, G. D. Edossa, and B. A. Gonfa, "Synthesis of zinc oxide nanoparticles using leaf extract of lippia adoensis (koseret) and evaluation of its antibacterial activity," *Journal of Chemistry*, vol. 1, p. 9, 2020.
- [21] P. Yadav, K. Lal, A. Kumar, S. K. Guru, S. Jaglan, and S. Bhushan, "Green synthesis and anticancer potential of chalcone linked-1, 2, 3-triazoles," *European Journal of Medicinal Chemistry*, vol. 126, pp. 944–953, 2017.
- [22] J. Zitko, O. Jand'ourek, P. Paterova et al., "Design, synthesis and antimycobacterial activity of hybrid molecules combining pyrazinamide with a 4-phenylthiazol-2-amine scaffold," *MedChemComm*, vol. 9, no. 4, pp. 685–696, 2018.
- [23] L. A. Illicachi, J. Montalvo-Acosta, A. Insuasty et al., "Synthesis and DFT calculations of novel vanillin-chalcones and their 3-Aryl-5-(4-(2-(dimethylamino)-ethoxy)-3-methoxyphenyl)-4, 5-dihydro-1H-pyrazole-1-carbaldehyde derivatives as anti-fungal agents," *Molecules*, vol. 22, no. 9, Article ID 1476, 2017.
- [24] J. Hudzicki, "Kirby-Bauer disk diffusion susceptibility test protocol," *American Society for Microbiology*, vol. 15, pp. 55–63, 2009.
- [25] D. H. Bergey, *Bergey's Manual of Determinative Bacteriology*, Lippincott Williams & Wilkins, Philadelphia, 1994.
- [26] J. N. Eloff, "Avoiding pitfalls in determining antimicrobial activity of plant extracts and publishing the results," *BMC Complementary and Alternative Medicine*, vol. 19, no. 1, pp. 106–108, 2019.
- [27] F. Ullah, N. Iqbal, M. Ayaz et al., "DPPH, ABTS free radical scavenging, antibacterial and phytochemical evaluation of crude methanolic extract and subsequent fractions of Chenopodium botrys aerial parts," *Pak J Pharm Sci*, vol. 30, no. 3, pp. 761–766, 2017.
- [28] R. R. Varma, J. G. Pandya, F. U. Vaidya, C. Pathak, B. S. Bhatt, and M. N. Patel, "Biological activities of pyrazoline-indole based Re (I) carbonyls: DNA interaction, antibacterial, anticancer, ROS production, lipid peroxidation, in vivo and in vitro cytotoxicity studies," *Chemico-Biological Interactions*, vol. 330, Article ID 109231, 2020.
- [29] P. Sailaja Rao, S. Kalva, A. Yerramilli, and S. Mamidi, "Free radicals and tissue damage role of antioxidants," *Free Radicals and Antioxidants*, vol. 1, no. 4, pp. 2–7, 2011.
- [30] D. F. Veber, S. R. Johnson, H. Y. Cheng, B. R. Smith, K. W. Ward, and K. D. Kopple, "Molecular properties that influence the oral bioavailability of drug candidates," *Journal of Medicinal Chemistry*, vol. 45, no. 12, 2002.
- [31] A. Daina, O. Michielin, and V. Zoete, "SwissADME: a free web tool to evaluate pharmacokinetics, drug-likeness and medicinal chemistry friendliness of small molecules," *Scientific Reports*, vol. 7, no. 1, 2017.
- [32] A. Ah and A. Yi, "In silico pharmacokinetics and molecular docking studies of lead compounds derived from Diospyros mespiliformis," *PharmaTutor*, vol. 7, no. 3, pp. 31–37, 2019.
- [33] D. Seeliger and B. L. de Groot, "Ligand docking and binding site analysis with PyMOL and Autodock/Vina," *Journal of Computer-Aided Molecular Design*, vol. 24, no. 5, pp. 417–422, 2010.
- [34] O. Trott, A. J. Olson, and A. D. Vina, "AutoDock Vina improving the speed and accuracy of docking with a new scoring function, efficient optimization, and multithreading," *Journal of Computational Chemistry*, vol. 31, no. 2, pp. 455–461, 2010.
- [35] G. Jones, P. Willett, R. C. Glen, A. R. Leach, and R. Taylor, "Development and validation of a genetic algorithm for flexible docking 1 Edited by F. E. Cohen," *Journal of Molecular Biology*, vol. 267, no. 3, pp. 727–748, 1997.
- [36] M. J. Piltan and J. S. Ghomi, "Nano crystalline ZnO catalyzed one pot three-component synthesis of 7-alkyl-6H, 7H-naphtho [1', 2': 5, 6] pyrano [3, 2-c] chromen-6-ones under solvent-free conditions," *Bulletin of the Chemical Society of Ethiopia*, vol. 30, no. 2, pp. 289–296, 2016.
- [37] A. Aldalbahi, S. Alterary, R. Ali Abdullrahman Almoghim et al., "Greener synthesis of zinc oxide nanoparticles: characterization and multifaceted applications," *Molecules*, vol. 25, no. 18, Article ID 4198, 2020.
- [38] A. M. Pillai, V. S. Sivasankarapillai, A. Rahdar et al., "Green synthesis and characterization of zinc oxide nanoparticles with antibacterial and antifungal activity," *Journal of Molecular Structure*, vol. 1211, Article ID 128107, 2020.
- [39] M. Rani and Y. Mohamad, "Synthesis, studies and in vitro antibacterial activity of some 5-(thiophene-2-yl)-phenyl pyrazoline derivatives," *Journal of Saudi Chemical Society*, vol. 18, no. 5, pp. 411–417, 2014.
- [40] M. A. K. Shakhathreh, M. L. Al-Smadi, O. F. Khabour, F. A. Shuaibu, E. I. Hussein, and K. H. Alzoubi, "Study of the antibacterial and antifungal activities of synthetic benzyl

- bromides, ketones, and corresponding chalcone derivatives,” *Drug Design, Development and Therapy*, vol. 10, 2016.
- [41] M. S. Shah, M. M. Rahman, M. D. Islam et al., “Synthesis, antimicrobial and antioxidant evaluation with in silico studies of new thiazole Schiff base derivatives,” *Journal of Molecular Structure*, vol. 1248, Article ID 131465, 2022.
- [42] P. Abishad, P. Niveditha, V. Unni et al., “In silico molecular docking and in vitro antimicrobial efficacy of phytochemicals against multi-drug-resistant enteroaggregative *Escherichia coli* and non-typhoidal *Salmonella* spp,” *Gut Pathogens*, vol. 13, no. 1, pp. 46–11, 2021.
- [43] T. S. Ibrahim, A. J. Almalki, A. H. Moustafa et al., “Novel 1, 2, 4-oxadiazole-chalcone/oxime hybrids as potential antibacterial DNA gyrase inhibitors: design, synthesis, ADMET prediction and molecular docking study,” *Bioorganic Chemistry*, vol. 111, Article ID 104885, 2021.
- [44] C. A. Lipinski, F. Lombardo, B. W. Dominy, and P. J. Feeney, “Experimental and computational approaches to estimate solubility and permeability in drug discovery and development settings,” *Advanced Drug Delivery Reviews*, vol. 23, no. 1-3, pp. 3–25, 1997.
- [45] S. Lee, “The PreADME Approach: web-based program for rapid prediction of physico-chemical, drug absorption and drug-like properties,” 2003, [https://www.researchgate.net/publication/309311638\\_The\\_PreADME\\_Approach\\_Web-based\\_program\\_for\\_rapid\\_prediction\\_of\\_physico-chemical\\_drug\\_absorption\\_and\\_drug-like\\_properties](https://www.researchgate.net/publication/309311638_The_PreADME_Approach_Web-based_program_for_rapid_prediction_of_physico-chemical_drug_absorption_and_drug-like_properties).
- [46] S. Ghosh, “In silico study by using ProTox-II webserver for oral acute toxicity, organ toxicity, immunotoxicity, genetic toxicity endpoints, nuclear receptor signalling and stress response pathways of synthetic pyrethroids,” *World Scientific News*, vol. 132, pp. 35–51, 2019.
- [47] P. Banerjee, A. O. Eckert, A. K. Schrey, and R. Preissner, “ProTox-II a webserver for the prediction of toxicity of chemicals,” *Nucleic Acids Research*, vol. 46, no. W1, 2018.
- [48] Y. C. Martin, “A bioavailability score,” *Journal of Medicinal Chemistry*, vol. 48, no. 9, 2005.
- [49] P. Ertl, B. Rohde, and P. Selzer, “Fast calculation of molecular polar surface area as a sum of fragment-based contributions and its application to the prediction of drug transport properties,” *Journal of Medicinal Chemistry*, vol. 43, no. 20, 2000.
- [50] C. Alonso, V. Carrer, S. Espinosa et al., “Prediction of the skin permeability of topical drugs using in silico and in vitro models,” *European Journal of Pharmaceutical Sciences*, vol. 136, Article ID 104945, 2019.
- [51] A. Finch and P. Pillans, “P-glycoprotein and its role in drug-drug interactions,” *Aust Prescr*, vol. 37, no. 4, pp. 137–139, 2014.
- [52] M. R. Goswami, “An easy screening through in silico study for predictive toxicity mechanisms of different phthalate compounds by using online tool (Protox-II webserver),” *Journal of Advanced Scientific Research*, vol. 10, no. 04 Suppl 2, pp. 246–253, 2019.
- [53] M. N. Drwal, P. Banerjee, M. Dunkel, M. R. Wettig, and R. Preissner, “ProTox a web server for the in silico prediction of rodent oral toxicity,” *Nucleic Acids Research*, vol. 42, no. W1, pp. W53–W58, 2014.
- [54] M. A. Islam and T. S. Pillay, “Identification of promising anti-DNA gyrase antibacterial compounds using de novo design, molecular docking and molecular dynamics studies,” *Journal of Biomolecular Structure and Dynamics*, vol. 38, no. 6, 2020.
- [55] A. Daina and V. Zoete, “A boiled-egg to predict gastrointestinal absorption and brain penetration of small molecules,” *ChemMedChem*, vol. 11, no. 11, 2016.
- [56] T. Hillman, “Reducing bacterial antibiotic resistance by targeting bacterial metabolic pathways and disrupting RND efflux pump activity,” *Iberoamerican Journal of Medicine*, vol. 4, no. 1, pp. 60–74, 2022.
- [57] M. Durcik, Z. Skok, J. Ilas et al., “Hybrid inhibitors of DNA gyrase A and B design, synthesis and evaluation,” *Pharmaceutics*, vol. 13, no. 1, p. 6, 2020.
- [58] C. Ji, I. Sharma, D. Pratihari et al., “Designed small-molecule inhibitors of the anthranilyl-CoA synthetase PqsA block quinolone biosynthesis in *Pseudomonas aeruginosa*,” *ACS Chemical Biology*, vol. 14, no. 6, 2019.
- [59] M. T. El Sayed, A. E. Sarhan, E. Ahmed et al., “Novel pyruvate kinase (PK) inhibitors: new target to overcome bacterial resistance,” *ChemistrySelect*, vol. 5, no. 11, 2020.
- [60] N. S. Kumar, E. M. Dullaghan, B. B. Finlay et al., “Discovery and optimization of a new class of pyruvate kinase inhibitors as potential therapeutics for the treatment of methicillin-resistant *Staphylococcus aureus* infections,” *Bioorganic and Medicinal Chemistry*, vol. 22, no. 5, 2014.
- [61] Y. Wang, B. Liu, D. Grenier, and L. Yi, “Regulatory mechanisms of the LuxS/AI-2 system and bacterial resistance,” *Antimicrobial Agents and Chemotherapy*, vol. 63, no. 10, 2019.
- [62] S. N. Radyuk, K. Michalak, V. Klichko et al., “Peroxiredoxin 5 confers protection against oxidative stress and apoptosis and also promotes longevity in *Drosophila*,” *Biochemical Journal*, vol. 419, no. 2, pp. 437–445, 2009.